ADVANCED HEALTHCARE MATERIALS
www.advhealthmat.de

Citrate-Based Fluorescent Biomaterials

*Dingying Shan, Jer-Tsong Hsieh, Xiaochun Bai, and Jian Yang**

Fluorescence imaging has emerged as a promising technique for monitoring and assessing various biologically relevant species in cells and organisms, driving the demand for effective fluorescent agents with good biocompatibility and high fluorescence performance. However, traditional fluorescent agents, such as quantum dots (QDs) and organic dyes, either suffer from toxicity concerns or poor fluorescence performance (e.g., low photobleaching-resistance). In this regard, citrate-based fluorescent biomaterials, which are synthesized from the natural and biocompatible precursor of citric acid (CA), have become competitive alternatives for fluorescence imaging owing to their biocompatibility, cost effectiveness, straightforward synthetic routes, flexible designability, as well as strong fluorescence with adjustable excitation/emission wavelengths. Accordingly, numerous citrate-based biomaterials, including carbon dots (CDs), biodegradable photoluminescent polymers (BPLPs), and small molecular fluorophores, have been developed and researched in the past few decades. This review discusses recent progress in the research and development of citrate-based fluorescent materials with emphasis on their design and synthesis considerations, material properties, fluorescence properties and mechanisms, as well as biomedical applications. It is expected that this review will provide an insightful discussion on the citrate-based fluorescent biomaterials, and lead to innovations for the next generation of fluorescent biomaterials and fluorescence-based biomedical technology.

1. Introduction

Advances in imaging techniques could provide diagnoses and treatments of various diseases, defects, and cancers in a more safe and more effective way.[1] Among imaging techniques applied clinically, of particular interest is fluorescence imaging, which demonstrates the advantageous properties of high sensitivity, high temporal resolution, cost effectiveness, and ease of use.[2] Traditional fluorescence imaging, due to their limited imaging depth, have been mostly confined to in vitro applications such as cell labeling, immunohistochemistry, and flow cytometry. However, recent development of advanced fluorescent agents with longer excitation/emission wavelengths [e.g., near-infrared (NIR)] has boosted the ability of fluorescence imaging to penetrate deeper into tissues, thus greatly improving the viability of fluorescence imaging for in vivo applications.[3] To date, the major fluorescent agents in use have been fluorescent organic dyes, quantum dots (QDs), and fluorescent proteins, all of which are hampered by drawbacks that must be overcome.[4] For example, most organic dyes such as fluorescein, rhodamine, and cyanine exhibit poor photostability and low dye-to-reporter molecule labeling ratios, which limit their imaging efficiency.[5] QDs, which have been extensively studied in fluorescence-based bioapplications such as in vitro cellular labeling and in vivo bioimaging,[6] are often toxic as they consist of metal complexes.[7] Fluorescent proteins also suffer from limited varieties, photobleaching and instability.[8] Given the numerous shortcomings of existing fluorescence imaging agents, there is an urgent need for biocompatible and/or biodegradable materials with high fluorescence performance to spearhead the next generation of fluorescence imaging resources that will open the door to new opportunities in modern medical care.

To satisfy the need for biocompatible fluorescence materials, biocompatible resources have gained great attention as precursors for fluorescent materials synthesis. Citric acid (CA) is an organic acid that is naturally present in citrus fruits and serves as an intermediate in the citric acid cycle that occurs in the metabolism of all aerobic organisms. Combined with its high reactivity effected by the presence of one hydroxyl and three carboxyl groups, CA has become one of the most frequently used molecules for the synthesis of biocompatible fluorescent materials. Citrate-based fluorescent materials were first reported in the 19th century by W. J. Sell and T. H. Easterfield. In their trailblazing study, fluorescent citrazinic acid was formed as a result of condensation between CA and ammonia.[9] Almost a hundred years later, fluorescent five-membered ring fused 2-pyridones were synthesized by reacting CA with D-penicillamine[10] and

D. Shan, Prof. J. Yang
Department of Biomedical Engineering
Materials Research Institute
The Huck Institutes of The Life Sciences
The Pennsylvania State University
University Park, PA 16802, USA
E-mail: jxy30@psu.edu
Prof. J. T. Hsieh
Department of Urology
The University of Texas Southwestern Medical Center
Dallas, TX 75390, USA
Prof. X. Bai
Department of Cell Biology
School of Basic Medical Sciences
Southern Medical University
Guangzhou 510515, China

DOI: 10.1002/adhm.201800532

o-amino-thiophenol.[11] Since the accidental discovery of fluorescent carbon dots (CDs) during the electrophoretic purification of single-walled carbon nanotubes in 2004,[12] CA has become one of the most popular carbon sources applied in the development of fluorescent CDs.[13–17] These citrate-based CDs, when compared with traditional fluorescent agents, possess numerous advantages, including biocompatibility, straightforward synthesis, and strong fluorescence with adjustable emission spectra (from blue to NIR).[18–22] Researchers have proposed that the fluorescence performance of citrate-based CDs may be attributed to both their carbon cores and small molecular fluorophores.[23–28] Later, Yang and co-workers discovered a family of citrate-based polymers,[29,30] among which a set of biodegradable photoluminescent polymers (BPLPs) were developed with fluorophores formed by reacting CA and amine-containing molecules including amino acids.[31,32] BPLPs demonstrated in vitro cytocompatibility, minimal in vivo chronic inflammatory responses, controlled degradability, desired mechanical properties, excellent processability for micro-/nanofabrication, as well as strong and adjustable fluorescence.[31–35] Recently, due to the importance of small molecular fluorophores formed by CA and amine based molecules, various citrate-based fluorescent molecules have also been developed.[34,36–38]

The developed citrate-based fluorescent materials, which included CDs, BPLPs, and molecular fluorophores, presented favorable biocompatibility/biodegradability, and strong and stable fluorescence, enabling their use in important biomedical applications, such as bioimaging,[33,35,39–45] biosensing,[39,46–50] and nanomedicine.[51–53] For example, NIR-imaging information encryption and in vivo NIR fluorescence imaging of the stomach of a living mouse were achieved using citrate-based CDs synthesized from CA and urea.[54] Using the BPLPLs, an immune cell-mediated nanoparticle targeting drug delivery system was created and demonstrated significant theranostic effects.[53] Moreover, molecular fluorophore synthesized from CA and cysteine (CA-Cys) was applied as selective chloride sensors, and a smartphone operated chloridometer was further designed for the diagnosis of cystic fibrosis (CF).[50,55] Overall, the development of citrate-based fluorescent materials in current studies has played a significant role in theranostic healthcare and regenerative engineering. This review will provide a comprehensive discussion of the design and synthesis strategies, material properties, fluorescence properties, and mechanisms, as well as biomedical applications of various citrate-based fluorescent materials, including CDs, BPLPs, and molecular fluorophores (**Figure 1**).

Dingying Shan received her B.S. degree in biomaterials and M.S. degree in chemistry from Beijing University of Chemical Technology, China. She is currently a Ph.D. student at the Pennsylvania State University under the supervision of Prof. Jian Yang. Her research work is focusing on the development of biodegradable citrate-based polymers for bioimaging, tissue engineering, drug delivery, and bioelectronics applications.

Jian Yang is a full professor in the Department of Biomedical Engineering at the Pennsylvania State University. He received his Ph.D. in polymer chemistry and physics in 2002 at the Institute of Chemistry, the Chinese Academy of Sciences in Beijing, China, and then received his postdoctoral training at Northwestern University (Evanston, IL) in 2003–2006. Prof. Yang was the first to report citrate-based biodegradable photoluminescent polymers. His research interests lie in biomaterials, tissue engineering, drug delivery, bioimaging and biosensing.

2. Citrate-Based Carbon Dots

CDs are a new class of carbon nanomaterials with sizes below 10 nm, which have drawn intensive attention since their first discovery due to their unique physical and chemical properties.[16,56] CDs were considered as great alternatives to cytotoxic QDs due to their biocompatibility, low cost, and similar fluorescence properties to QDs. CDs can be synthesized from carbon sources with (passivated CDs) or without passivation/doping agents ("naked" CDs). Among all the carbon sources for CDs preparation, such as glucose, glycerol, sucrose, CA, and malic acid, which have been applied for CDs preparation, CA has become one of the most popular carbon source as it has three reactive carboxyl groups to provide sufficient dehydration, carbonization, and interaction with passivation/doping agents.[57] Citrate-based CDs could be prepared by reacting CA with or without various small organic molecules based passivation/doping agents, including urea, 1,2-ethylenediamine (EDA) and amino acids. Owing to their various advantages, such as facile synthesis, good biocompatibility, and favorable fluorescence performance, citrate-based CDs offer great potential in biomedical applications.

2.1. Preparation Methods for Citrate-based CDs

2.1.1. Thermal Decomposition

Thermal decomposition, which directly applies external heat to cause dehydration and carbonization of CA and other molecular precursors, is a facile method used to synthesize citrate-based CDs. The advantages provided by this method include low cost, short reaction time, solvent-free process, and ready scalability.[22,26,49,58] With thermal decomposition, CA could work as the sole precursor to prepare CDs. For instance, Dong et al. synthesized CDs by

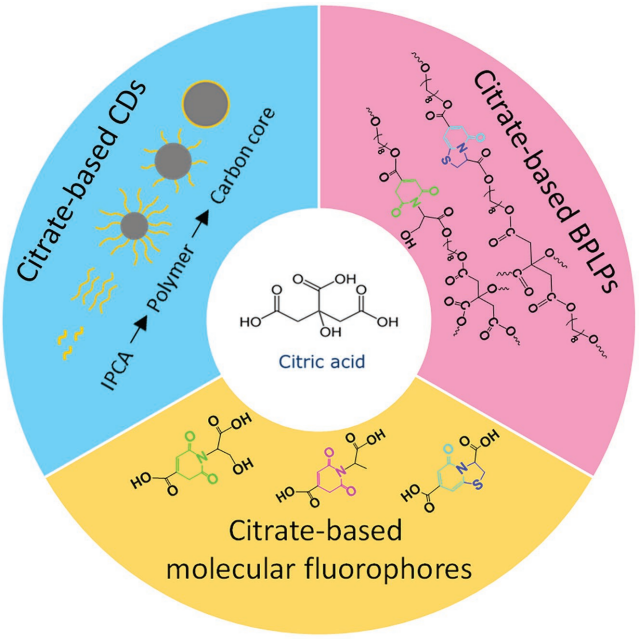

Figure 1. Citrate-based fluorescent biomaterials.

heating CA placed inside a beaker with a heating mantle at 200 °C for 30 min.[22] The resulting CDs were in the form of nanosheets that had width of ≈15 nm and thickness of 0.5–2.0 nm. These CDs presented a strong and excitation-independent blue fluorescence. Furthermore, Wang et al. prepared highly fluorescent organosilane-functionalized CDs, with quantum yield (QY) of 47% using straightforward pyrolysis of CA and *N*-(*β*-aminoethyl)-*γ*-aminopropyl methyldimethoxy silane (AEAPMS) at 240 °C for 1 min.[58] The obtained CDs with a diameter of ≈0.9 nm were then fabricated into films and monoliths using a simple heating process at 80 °C for 24 h. Through hydrolyzing and cocondensing the CDs with silica, water dispersible and biocompatible silica-encapsulated CDs (CDs/silica) with the size of about 12 nm were manufactured, offering the potential for biolabeling and imaging applications.

2.1.2. Microwave Irradiation

Microwave, a type of electromagnetic radiation, possesses a broad wavelength ranging from 1 mm to 1 m, and provides effective and homogeneous heating for the synthesis of citrate-based CDs.[23,42,59,60] Zhai et al. reported a one-step microwave pyrolysis approach to synthesize luminescent CDs from CA and various amines, including 1,2-ethylenediamine (EDA), diethylamine (DEA), triethylamine (TEA), and 1,4-butanediamine (BDA).[59] In their study, the authors demonstrated that all the resulting CDs (EDA-CDs, DEA-CDs, TEA-CDs, and BDA-CDs) presented enhanced fluorescence performance when compared to N-free CDs. They also found that an optimum microwave time of 2 min, and an optimal amino group/carboxyl group ratio of 2:3, produced CDs with the strongest fluorescence emissions. Among all the CDs, EDA-CDs exhibited the best fluorescence performance with a QY of 30.2%. Interestingly, EDA-CDs exhibited an excitation-dependent fluorescence emission (460–530 nm) when the excitation wavelength ranged from 400 to 460 nm, while an excitation-independent fluorescence behavior (460 nm) was exhibited when the excitation wavelength measured shorter than 400 nm (tested excitation wavelength: 320–400 nm). Later, Bhaisare et al. synthesized jellylike CDs with CA and tetraoctylammonium bromide (TOAB) using microwave assisted heating (at maximum 500 W).[60] Four unique CA to TOAB ratios (5 g CA: 2/4/6/8 mL of 0.1 M TOAB) were applied in the synthesis, with the obtained CDs named as C-dots I, II, III, and IV, respectively. The authors also reported that an optimum reaction time of 2–3 min produced the desired yellowish CDs. It turned out that C-dots IV demonstrated the highest QY of 11%, and exhibited excitation-dependent and decreased emissions (350–600 nm) when the excitation wavelength increased from 300 to 460 nm.

2.1.3. Hydrothermal Treatment

Hydrothermal treatment, which typically causes organic precursors to react in a hydrothermal reactor at high temperature, is a low cost, nontoxic, and environmentally friendly process to prepare CDs.[18,48,61] Accordingly, many citrate-based CDs were synthesized using hydrothermal treatments. For instance, Dong et al. prepared nitrogen and sulfur codoped CDs (N,S-CDs) from CA and L-cysteine using a one-step hydrothermal treatment.[18] The obtained N,S-CDs had a nanosheet structure with an average height of 2 nm and an average width of 8 nm. The N,S-CDs displayed high QY of 73% and excitation-independent emission (415 nm) under excitation wavelength from 285 to 405 nm. Combined with their low cytotoxicity, these N,S-CDs will serve as great candidates for bioimaging applications. Furthermore, Zhang et al. also developed nitrogen-doped (N-doped) CDs by processing CA and urea through a hydrothermal treatment heated in a stainless steel autoclave at 200 °C for 10 h.[48] The resulting N-doped CDs had a narrow distribution with an average diameter of about 5.23 nm, and presented an excitation-dependent fluorescence emission with a QY of 25.4%.

2.1.4. Solvothermal Treatment

Solvothermal treatment is another approach for CDs preparation, in which organic precursors are subjected to thermal treatment in organic solvents. Tian et al. prepared full-color emissive CDs by processing CA and urea through a solvothermal treatment, which employed three different solvents (water, glycerol, and dimethylformamide (DMF)) and their combinations.[62] By adjusting the volume ratios of water, glycerol, and DMF (1:0:0, 1:1:0, 1:3:0, 0:1:0, 0:4:1, 0:3:1, 0:0:1), the respective solutions of the resulting CDs displayed bright fluorescence emissions that covered the whole light spectral ranging from blue to red under the excitation of UV light. The authors also incorporated CDs into a silica network to prevent aggregation of CDs, resulting in strong full-colored CDs with fluorescence QY of 30–40%. In addition, Miao et al. synthesized multiple color emissive CDs using CA and urea in dimethylformamide (DMF) by controlling the molar ratio of CA to urea (0–1.0) in order to adjust the surface function degree and adjusting reaction temperature (140–200 °C) that in turn allowed the modification of the extent

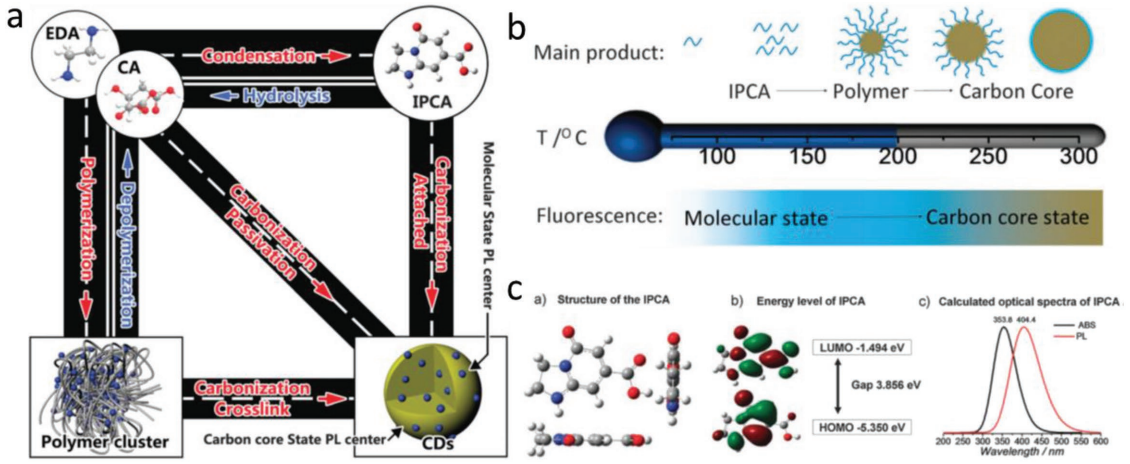

Figure 2. Structure properties of citrate-based CDs. a) A schematic of the relationship between different products in CDs. b) A schematic of the CDs obtained at different hydrothermal temperatures. c) The results from Gaussian calculation: (ca) the structure of IPCA. (cb) Frontier orbital energy of IPCA. (cc) Calculated Abs and PL spectra of IPCA. Reproduced with permission.[27] Copyright 2015, the Royal Society of Chemistry.

of graphitization.[19] Due to the regulation of reaction conditions, the obtained CDs displayed fluorescence emission light that ranged from blue to red, covering almost the entire light spectrum (430–630 nm). The relative fluorescence QY of the CDs with blue, green, and red emissions were 52.6%, 35.1%, and 12.9%, respectively.

2.2. Structure and Material Properties of Citrate based CDs

2.2.1. Polydispersity in Structures and Properties

The structures of citrate-based CDs are heavily influenced by synthesis conditions, such as reaction temperature, reaction time, precursor ratios, solvent and pH. Employing a one-pot synthesis strategy, the obtained citrate-based CDs typically had polydispersed structures, including small molecules, oligomers, polymer chains, polymer clusters, and carbon cores.[14,15,27,28] Song et al. systematically studied the components of CDs synthesized from CA and ethylenediamine (EDA) (**Figure 2**).[27] They separated the CDs reacted at 140 °C by column chromatography on silica, and obtained 5 batches of fluorescent components. The molecular structure of batch 1 was confirmed as a fluorescent molecule (imidazo[1,2-*a*] pyridine-7-carboxylic acid, 1,2,3,5-tetrahydro-5-oxo-, IPCA), which had a molecular weight of 180 g mol^{-1}. Characterizations showed that the aqueous solution of IPCA exhibited a strong excitation-independent blue fluorescence with a high QY (85.84%) but low photostability. It also had a molar extinction coefficient of 3780 M^{-1} cm^{-1} and a lifetime of ≈14.06 ns. Batches 2 and 3 mainly contained oligomers (dimers, trimers, and tetramers), a result which was confirmed by liquid chromatography–mass spectra (LC–MS). Batches 4 and 5 were regarded as nanosized carbon cores that resulted from the polymerization of monomers and carbonization of CA.[22] Characterization indicated that IPCA was the main contributor to the strong fluorescence property of CDs, while carbon cores were responsible for the excitation-dependent behaviors of CDs. Moreover, chemical equilibriums existed among the starting molecules, IPCA, polymer clusters and carbons core in the hydrothermal process. The quality and composition of CDs were influenced by multiple factors, including reaction temperature, initial starting material molar ratios, and initial pH values. The authors believed that the different components in the CDs worked together to produce synergistic effects. For example, the polymer clusters and carbon cores interact with IPCA to improve its water solubility and stability, enabling higher efficiency for practical applications. Moreover, Deng et al. developed an ultracentrifugation approach using a hydrophilicity gradient to separate nonsedimental CDs.[63] Practically, the CDs were synthesized from CA and ethylenediamine (EDA) and then treated with acetone to form clusters. Solutions of DI water in ethanol with decreasing volume ratios (50%, 40%, 30%, and 20% water/ethanol) were used as the separation-layer gradient. During the subsequent separation process, the preaggregated CDs were divided into groups with differing carbonization degrees and sizes. The exact group that CDs were divided into depended on the differences in hydrophilicity and solubility of the centrifugal fractions. Depending on the characterization of size, composition, and fluorescence properties of CDs in each fraction, the authors found that the fluorescence of the CDs were mainly determined by their surface molecular state rather than size. In addition to the above examples, the polydipersity of CDs were found to be supported by the wide size distribution according to Transmission Electron Microscopy (TEM) and dynamic light scattering (DLS) analysis as well as broad peaks in NMR and mass spectra results.[15]

2.2.2. Abundant Reactive Groups

Due to the chemical properties of their precursors, citrate-based CDs contain plentiful reactive and modifiable groups and short polymer chains in their system after incomplete carbonization, enabling further modification through absorbing/conjugating

functional structures. For instance, Goh et al. developed hyaluronic acid (HA)-CD conjugates for in vivo real-time imaging of target-specific delivery of HA.[64] Practically, the conjugates were prepared by using EDC to conjugate polyethylene glycol (PEG) diamine capped CDs onto HA derivatives. Zheng et al. also created a multifunctional theranostic agent (CD-Oxa) by conjugating an anticancer agent (oxidized oxaliplatin, Oxa(IV)-COOH) onto the surface of citrate-based CDs.[65] In detail, CA and polyene polyamine (PEPA) were used as precursors to synthesize the CDs that were surface modified with $-NH_2$, and then Oxa(IV)-COOH was conjugated to CDs surface through EDC/NHS chemistry.

2.3. Fluorescence Properties and Mechanisms of Citrate based CDs

2.3.1. Fluorescence Properties

The fluorescence properties of citrate-based CDs varied with preparation conditions, including variation in precursor types, precursor ratios, synthesis temperatures, synthesis time, pH, doping and/or surface passivation, and solvents.[25,26,66,67] Qu et al. designed and synthesized a series of citrate-based CDs via hydrothermal method and investigated different impact factors to determine the fluorescence performance of the resulting CDs.[67] They first synthesized CDs from CA under a basic reaction condition (NaOH). The obtained CDs demonstrated excitation-independent strong blue emission at 450 nm under excitation of 340–400 nm; relatively low QY of 22%, and single exponential lifetime of 7 ns. Then urea was utilized as an N-dopant to react with CA at different times (2, 4, 6, 8, and 24 h) to prepare N-doped CDs. All the resulting CDs displayed narrow fluorescence emission band at 450 nm with the same lifetime of 8 ns but increased QYs of 58%, 78%, 80%, 81%, and 82%, respectively, suggesting the extent of N-doping effectively improved the fluorescence performance of CDs. Later, the authors studied the influence of amines types, such as ternary (hexamethylene tetraamine (HMTA)), secondary (diethylene amine (DEA)), and primary amines (ethanol amine (EA)), on the fluorescence properties of citrate-based CDs. The obtained three CDs, which were synthesized from CA and HMTA/DEA/EA, had close structures and similar optical properties, with increased QY of 20%, 30%, and 36%, and lifetimes of 10, 7, and 6 ns, respectively. However, when ethylene diamine (EDA) was applied to react with CA, the resulting CDs exhibited a high fluorescence QY of 94% and a long lifetime of 14 ns due to the higher doping degree of diamine when compared to monoamine. Beyond the investigation on various amines, the authors also investigated the influence of reaction time and temperature of fluorescence QY, and optimized the reaction conditions of CA and EDA reaction in order to obtain high QY of the N-doped CDs.

Other researchers have tried different approaches to adjust fluorescence emission to longer wavelengths. Qu et al. developed citrate-based CDs with green emission by modulating N-dopant precursor ratios.[20] In their study, the CDs prepared with the low urea/CA mass ratio of 0.2:1 exhibited the strongest blue emission at 440 nm under 360 nm excitation with a QY of 15% (higher than the QY (3%) of CDs synthesized solely from CA with the same method) and a lifetime of 9.0 ns. After increasing the urea/CA mass ratio to 2:1, the CDs ethanol aqueous solution presented strong green emission at 526 nm under 420 nm excitation with a higher QY of 36% and longer lifetime of 10.2 ns, enabling a green lasing emission in a linear long Fabry–Perot cavity. Later, Qu et al. also prepared citrate-based CDs with efficient orange emission from CA and urea through a solvothermal method with surface charges engineering.[68] Specifically, CA and urea were first reacted at 160 °C under solvothermal condition in DMF, and then treated with alkali (NaOH or KOH) aqueous solution for metal-cation-functionalization. The obtained CDs ethanol solution exhibited high fluorescence emission at 580 nm under 540 nm excitation, with a QY of 46%. In addition, Sun et al. prepared red emissive citrate-based CDs through microwave-assisted heating of CA in formamide.[69] The resulting red emissive CDs presented many attractive properties, including high QY of 22.9%, high photostability, broad absorption, two photon excitation fluorescence, cytocompatibility, and high photothermal conversion efficiency, which made them promising in nanomedicine and medical devices. Furthermore, Tian et al. created full-color emissive CDs from CA and urea through applying three different solvents, including water, glycerol, and dimethylformamide (DMF), and their combinations with a solvothermal method. Under UV light, the resulting CD solutions exhibited bright fluorescence from blue to red colors with the emission peaks gradually shifting from 448 nm to 453, 465, 550, 578, 583, and finally 638 nm for samples synthesized in selected volume ratios of water, glycerol, and DMF (1:0:0, 1:1:0, 1:3:0, 0:1:0, 0:4:1, 0:3:1, and 0:0:1).[62] Recently, Li et al. developed citrate-based CDs with near-infrared (NIR) excitation/emission and multiphoton-induced fluorescence through the surface engineering of CDs.[54] Practically, the CDs were first synthesized from CA and urea in DMF at 160 °C for 6h in an autoclave, and then treated with NaOH and HCl aqueous solutions. To obtain CDs with NIR excitation/emission, the as-synthesized CD powders were further modified with molecules or polymers rich in electron-acceptor groups (S=O/C=O), such as DMSO, DMF, NMP, and poly(vinylpyrrolidone) (PVP). After being treated with DMSO, the CDs exhibited efficient NIR emission at 760 nm under the excitation of 732 nm, with a PL QY of 10%. In vivo noninvasive NIR fluorescence bioimaging of the stomach of a living mouse was also conducted using PVP modified CDs. In addition, two-photon and three-photon induced fluorescence emission were achieved by DMSO modified CDs under excitation by a femtosecond pulse laser in the NIR-II window (1000–1700 nm). Overall, the current studies have provided rational design and preparation approaches for construction and clinical applications of citrate-based CDs derived imaging agents.

2.3.2. Fluorescence Mechanisms

As discussed in Section 2.2.1, citrate based CDs are complex systems with high polydispersity in structures, including small molecular fluorophores, oligomers, polymer chains, polymer clusters, and carbon cores. The structural variations that exist between each components of CDs play a role in determining differences in their fluorescence properties and mechanisms.

Multiple studies have demonstrated that molecular fluorophores exhibit strong fluorescence with high QY, while the carbon core state display weaker fluorescence with lower QY but better photostability vis-à-vis the molecule state.[24,27] Ultimately, the final fluorescence performance of CDs is a function of the fluorescence activities of all components. Although current understanding of the structural properties and fluorescence mechanisms of CDs remain inadequate, researchers have proposed a number of hypotheses to explain the fluorescence mechanism of CDs.[13–16,56,70,71] In the following section, we will discuss the fluorescence mechanisms of CDs, with focus on their three most important states (the molecule state, the carbon core state, and the surface state).

The Molecule State: At the early stages of the synthesis for citrate-based CDs, inter-/intramolecular dehydration and condensation reactions occur among precursors, and small organic molecules with strong excitation-independent fluorescence and high QY are formed. The molecular fluorophores mainly contain five or six-membered heterocyclic structures, which could be dissociated freely in solution or be connected on the surface and even interior of the carbon backbone.[28] When the synthesis proceeds to a higher temperature or longer time, the molecular fluorophores can be further dehydrated and/or carbonized to form polymer structures and carbon cores. Generally, the molecule state can easily be distinguished due to its unique characteristics, including a characteristic Gaussian peak in UV–vis spectra, and excitation-independent fluorescence emission. Many researchers have isolated the molecular fluorophores and investigated their structure properties and fluorescence performance.[23–27,67] Krysmann et al. first investigated the formation mechanism by pyrolysis of CA and ethanolamine (EA) precursor at various temperatures.[24] They pointed out that the strong fluorescence was mainly contributed by the molecular fluorophores at low pyrolysis temperature (180 °C). At higher pyrolysis temperatures, carbon cores were subsequently formed, and the fluorescence center of the system was gradually changed from molecular fluorophores to carbon cores. Later, Song et al. separated CDs made from CA and EDA through column chromatography, and successfully confirmed the existence of molecular fluorophore, referred as IPCA, by many characterizations.[27] The Gaussian calculations indicated that most of the atoms in IPCA stayed in the same plane with conjugated ring structures, which was regarded as the origin of the fluorescence of IPCA. The highest occupied molecular orbital (HOMO) band and lowest unoccupied molecular orbital (LUMO) band were calculated as −1.494 and −5.350 eV, respectively, and the predicted absorbance and fluorescence spectra was relatively consistent to the experiment results. The existence and fluorescence origin of the small molecules were further confirmed by Rogach and co-workers[25] and Kumbhakar and co-workers.[26] This mechanism of molecular fluorophores will later be expanded upon in Section 3.3.2.

The Carbon Core State: In the middle and later stages of the reaction process of preparing citrate-based CDs, further carbonization of precursors, molecular fluorophores, and the formed polymer clusters to form graphited carbon cores. Current studies indicate that the fluorescence emission of carbon cores is primarily related to the bandgap generated by the quantum confinement of the conjugated π-electrons in the sp^2 carbon,[72] which is attributed to the radiative recombination of electron-hole pairs of the delocalized π-electrons after the interaction between light and sp^2 carbon.[71,73] In actuality, the nanosized sp^2 aromatic structures are dispersed in a sp^3 nonconjugated carbon-oxygen matrix,[74] and the size of sp^2 domain and the ratio of sp^2/sp^3 affect the overall bandgap and thereby the fluorescence properties. Typically, an increase in sp^2 domain size decreases the π–π^* transition bandgap, causing the fluorescence emission to be red-shifted to a lower energy. Theoretical calculations indicated that the bandgap decreased to ≈2 eV in CDs with 20 aromatic rings compared to ≈7 eV for benzene.[75] Therefore, the fluorescence emission of CDs could be adjusted by changing the sp^2 domain size. Citrate-based CDs with full color fluorescence emission from blue to red, and the red-shifted fluorescence emission was consistent with increased sp^2 domain size.[20,21,54,62,68,76] To better understand the origin of the excitation-dependent fluorescence emission and the large Stoke-shift, Fu et al. developed a model system comprising three types of polycyclic aromatic hydrocarbon (PAH) molecules, including anthracene (3 rings), pyrene (4 rings), and perylene (5 rings), to represent the sp^2 nanodomains of carbon core state.[77] Their study suggested that the excitation-dependence of fluorescence emission was ascribed to the selective excitation of individual PAHs, and energy transfer from PAHs with larger energy gaps to those with smaller energy gaps caused a tail at longer wavelengths in the fluorescence emission. The authors also postulated that the large Stoke-shift was attributed to the self-trapping of an exciton in stacked PAH molecules.

The Surface State: The surface state is related to the synergistic hybridization of carbon backbone and various connected functional groups, leading to the recombination of electrons and holes. The energy gap of the surface state is regulated by the extent of the π-electrons and surface chemistry. Due to the existence of abundant active sites on surface, the surface state offers more possibilities to adjust the energy bands, thus tuning the fluorescence performances. For example, N and S codoped CDs synthesized from CA and L-cysteine had strong excitation-independent fluorescence emission with high QY (>70%), and presented better fluorescence performance when compared to that of CDs synthesized solely from CA (QY of 5.3%).[18] Qu et al. also found that increasing the N doping ratio could adjust the fluorescence emission from blue to green.[20] Pan et al. later reported truly fluorescent excitation-dependent CDs synthesized by CA and formamide. They demonstrated the blue light emissions of the CDs were attributed to aromatic structures, and the long-wavelength (green to red light) emissions arose from the existence of C—N/C—O and/or C—N bonds relevant functional groups.[66] More recently, Li et al. achieved enhanced NIR fluorescence emission from citrate-based CDs through surface modification with electron-acceptor groups, such as sulfoxide/carbonyl groups.[54]

As discussed above, a high ratio of π-conjugation based on planar aromatic ring structures are dispersed in CD systems, which lead to efficient fluorescence in diluted solutions. However, at high concentrated solutions and solid state, the fluorescence of unmodified CDs is usually weakened or quenched due to strong π–π stacking interactions among aromatic ring structures, referred to as ''aggregation-caused quenching'' (ACQ), which considerably hinders practical applications of CDs in

the fields of solid state optoelectronic devices and sensors. Currently, many studies have been performed to increase the steric hindrance among CD particles in order to alleviate the ACQ effect. For example, citrate-based CDs have been integrated with starch particles to prepare solid starch/CD composites that presented efficient fluorescence with a QY of ≈50%.[78] Moreover, surface modification of CDs with polymers and other organic molecules have been applied to reduce the ACQ effect. Using a facile microwave-assisted hydrothermal approach, Zheng et al. developed organosilane functionalized CDs (Si-CDs). The resulting solid Si-CDs demonstrated bright blue fluorescence with a high QY of 65.8%, and have been utilized to fabricate a white-light-emitting device.[79]

2.4. Biomedical Applications of Citrate based CDs

Owing to their exceptional advantages, which include biocompatibility, facile synthesis, and adjustable strong fluorescence performance, citrate-based CDs have recently drawn increasing attention for use in biomedical applications, such as bioimaging,[41,80] biosensing,[39,43] and biomedicine,[81] as described following.

2.4.1. Bioimaging

Abundant studies have been conducted to confirm both in vitro cell labeling and in vivo bioimaging capabilities of citrate-based CDs. To demonstrate the in vitro cell labeling capability of CDs, Bhaisare et al. developed a type of biocompatible CDs with excitation-dependent fluorescence from CA and tetraoctylammonium bromide, and applied these CDs to label HeLa cells under blue fluorescence.[60] Zholobak also applied CDs synthesized from CA and urea for live/fixed diploid epithelial swine testicular cell line (ST-cells) staining.[82] Furthermore, in vivo bioimaging was also conducted with citrate-based CDs. Goh et al. utilized citrate-based CDs for in vivo real time bioimaging of target-specific delivery of hyaluronic acid (HA) derivatives.[64] In detail, polyethylene glycol (PEG) diamine capped CDs were prepared through the pyrolysis of CA with PEG diamine. The HA-CD conjugates were later developed by conjugating CDs with HA through EDC. The resulting conjugates were employed for in vivo real-time tracking of target-specific delivery of HA to the liver, an organ that contains abundant HA receptors such as HARE and CD44. Recently, Yang et al. developed citrate-based CDs with red-shifted fluorescence under excitation at 530 nm through fluorine doping.[42] The obtained red-emissive fluorine doped CDs were later applied for both in vitro cell imaging and in vivo tumor imaging, demonstrating promising bioimaging potential for theranostic applications.

2.4.2. Biosensing

In addition to bioimaging, citrate-based CDs have also been widely applied for biosensing due to their favorable features that meet the expectations of biosensors, including biocompatibility, high sensitivity, easy operability, and low cost.[39,46,48,83] For instance, Zhang et al. synthesized from CA and urea a type of green CDs, which showed high fluorescence QY of 25.4%, good water solubility, and excellent photostability.[48] The green CDs showed significant and selective quenching by curcumin due to the inner filter effect. The developed sensors for curcumin detection with the citrate-based CDs presented a linear range of 2.0×10^{-7} to 1.0×10^{-5} mol L^{-1} and a detection limit of 8.48×10^{-8} mol L^{-1}. The sensor was also successfully applied for the detection of curcumin in urine samples and the recoveries were 95.71–103.81%. Later, Wang et al. developed N,S-doped CDs, which were synthesized from CA and L-cysteine, as a matrix for small molecule analysis by negative ion matrix assisted laser desorption/ionization (MALDI)-TOF MS.[81] The N,S-CDs matrix was employed for serum detection, quantitative characterization of endogenous glucose, and the classification of different subtypes of breast cancer cell lines. In these studies, various endogenous metabolites in serum were detected and two breast cancer cell lines were significantly distinguished by the newly designed CD matrix, indicating its great application potential for detecting complex biological samples. Moreover, Iqbal et al. developed citrate-based CDs with strong blue fluorescence (QY of 40% ± 0.06) from CA and melamine.[39] Hg (II) was able to quench the fluorescence of the CDs due to electrostatic interaction and electron transfer between Hg (II) and CDs, while GSH could recover the fluorescence of the CDs. Thus, the citrate-based CDs were employed as selective and sensitive sensor for turn on-off-on detection of Hg (II) and glutathione (GSH) with a detection limit as low as 20×10^{-9} and 40×10^{-9} M, respectively. Recently, multichannel fluorescence sensor arrays have been designed and fabricated using citrate-based CDs-metal ions ensembles. The resulting sensor arrays demonstrated excellent detection and discrimination of phosphate anions (e.g., ATP, ADP, AMP, PPi, and Pi) and a broad range of antibiotics.[84]

2.4.3. Biomedicine

Owing to their favorable biocompatibility, advanced bioimaging, and flexible chemical modification properties, citrate-based CDs have been employed for biomedicine applications. For example, Zheng et al. developed a multifunctional theranostic agent (CD-Oxa) by conjugating an anticancer agent (oxidized oxaliplatin, Oxa(IV)-COOH) onto the surface of citrate-based CDs.[65] Specifically, the citrate-based CDs that surface functionalized with $-NH_2$ were synthesized by thermal pyrolysis through CA and polyene polyamine (PEPA), and then the Oxa(IV)-COOH was conjugated with CDs through EDC/NHS chemistry. The resulting CD-Oxa integrated both the imaging properties of CDs and the anticancer function of oxaliplatin into a single unit. In vitro studies indicated that CD-Oxa possessed favorable biocompatibility, multicolor imaging ability, and anticancer effects. The CD-Oxa was also applied for in vivo bioimaging and liver tumor treatment. The results demonstrated that the CD-Oxa succeeded in killing tumor cells and tracking the distribution of the drugs. Overall, due to their reactive property, citrate-based CDs are able to achieve multiple functions, including drug delivery, dual/multiimaging modalities, and functional sensing.

3. Citrate-Based Biodegradable Photoluminescent Polymers

Biodegradable fluorescent polymers have attracted significant attentions in biomedical fields of theranostic and regenerative medicine.[85] Most of the reported fluorescent materials are made through the encapsulation or conjugation of fluorescent organic dyes[86] or inorganic QDs.[87] However, the low photostability of organic dyes and unacceptable toxicity of QDs have largely limited their applications and motivated the design of fully biodegradable and biocompatible fluorescent polymers. Benefitting from the reactive nature and ability to synthesize biocompatible molecular fluorophores of CA and amino acids, a series of citrate-based BPLPs were developed and applied.[31,32]

3.1. Design and Preparation of Citrate-based BPLPs

3.1.1. Citrate-Based Biodegradable Photoluminescent Prepolymers

Citrate-based BPLP prepolymers were prepared through a convenient and cost-effective thermal polycondensation reaction.[30–32,44,45,88] Typically, BPLP prepolymers were synthesized by reacting CA with one of the 20 natural amino acids and a biocompatible diol at 140 °C for several hours, which depends on the diol applied and the feeding ratios. In this reaction, CA and amino acids contributed to both the formation of molecular fluorophores and development of the polymer backbones, while the diol mainly aided the construction of polymer backbones. Because CA has multiple reaction groups (three carboxyl (−COOH) and one hydroxyl (−OH) groups), the obtained BPLPs presented branch structures and low molecular weight of about 1000 g mol^{-1} (further reaction would cause crosslinking). Both oil soluble and water soluble BPLP prepolymers were prepared through the application of aliphatic diols, such as 1,8-octanediol (OD), and hydrophilic diols, such as polyethylene glycol (PEG), respectively. All resulting BPLP prepolymers exhibited strong fluorescence which could be tuned by adjusting the amino acids, monomer feeding ratios, or even excitation. With a facile nanoprecipitation method, the oil soluble BPLP prepolymers were able to be fabricated into nanoparticles for bioimaging. In addition, due to pendant −COOH and −OH groups in BPLPs, they could be further polymerized into crosslinked elastomeric BPLPs (CBPLPs) in different forms, including films, scaffold, and hydrogels, or modified with various functionalities.

3.1.2. Chain Extension of Citrate-Based BPLP Prepolymers

Due to their low molecular weight, the above prepared sticky and honey-like BPLPs showed fast degradation and had weak mechanical properties, which significantly limited their potential for biomedical applications. Consequently, researchers have applied several chain extension approaches to adjust BPLPs' molecular weight, aiming to improve material's degradation profile and mechanical properties, as well as introduce new properties to BPLPs. Yi et al. developed a urethane-doped BPLP (UBPLP) by chain extension reaction of BPLP, which reacted from CA, L-cysteine/L-serine, and OD with a molar ratio of 1:0.2:1.1, using 1,6-hexamethyl diisocyanate (HDI) as a chain extender.[89] The obtained UBPLP demonstrated strong fluorescence (QY of 38.65%) and excellent cytocompatibility. Both UBPLP nanoparticles and crosslinked UBPLP scaffolds could be noninvasively detected in vivo. The crosslinked UBPLP also displayed soft and elastic, but strong mechanical properties. Another chain extension study was conducted using BPLPs to initiate ring-opening polymerization of lactones in the development of biodegradable photoluminescent polylactones (BPLPLs), including biodegradable photoluminescent poly-L-lactic acid (BPLP-PLLA)[35] and biodegradable photoluminescent polymer-poly(lactide-*co*-glycolide) (BPLP-PLGA).[33] The resulting BPLPLs exhibited similar thermal properties and biocompatibility to commercial polylactones, as well as tailored biodegradability. BPLPLs were also into different morphologies, such as films, nanoparticles, and porous scaffolds. The strong fluorescence property enabled BPLPLs to perform noninvasive fluorescence imaging for tracking the degradation of materials in vivo (**Figure 3**a). In addition to chain extension approaches, amphiphilic BPLPs (ABPLPs) were also investigated by reacting oil soluble BPLPs with hydrophilic components. For instance, oil soluble BPLPs, which was reacted from CA, L-cysteine, and poly(propylene glycol) (PPG) (molecular weight of 425, 725, and 2000), were conjugated with hydrophilic −COOH modified methoxy poly(ethylene glycol) (MPEG) (molecular weight of 750, 2000, and 5000) to prepare ABPLPs through DCC/DMAP chemistry.[44] With the resulting ABPLPs, nanosized micelles with strong fluorescence were fabricated and applied for both in vitro and in vivo bioimaging. Yang's lab used BPLP as a hydroxyl-terminated aliphatic polyol during the synthesis process of the waterborne polyurethane (WPU) to prepare another amphiphilic biodegradable photoluminescent WPU copolymer (BPLP-WPU). The resulting fluorescent BPLP-WPU were fabricated into stable nanomicelles and applied for tumor imaging and therapy.[51] Therefore, the chain extension of BPLPs could be an effective way to improve material properties of BPLPs as well as integrate intrinsic fluorescence properties into other biomaterials, significantly promoting the understanding, design, and use of biodegradable fluorescent polymers.

3.2. Material Properties of Citrate-Based BPLPs

3.2.1. Biodegradation

Degradation is a critical property of biomaterials since it affects mechanical performance, toxicity, material-tissue interaction, drug release, and many other properties. With hydrolysable ester and amide bonds, the citrate-based BPLPs were biodegradable in physiological conditions, and the degradation products were nontoxic because of the biocompatibility of monomers used for the preparation of BPLPs.[31] BPLP prepolymers exhibited relatively fast (generally within one month) but adjustable in vitro degradation profiles, depending on the monomer ratios and polymerization conditions. Crosslinked BPLP films had much slower degradation rates which could be

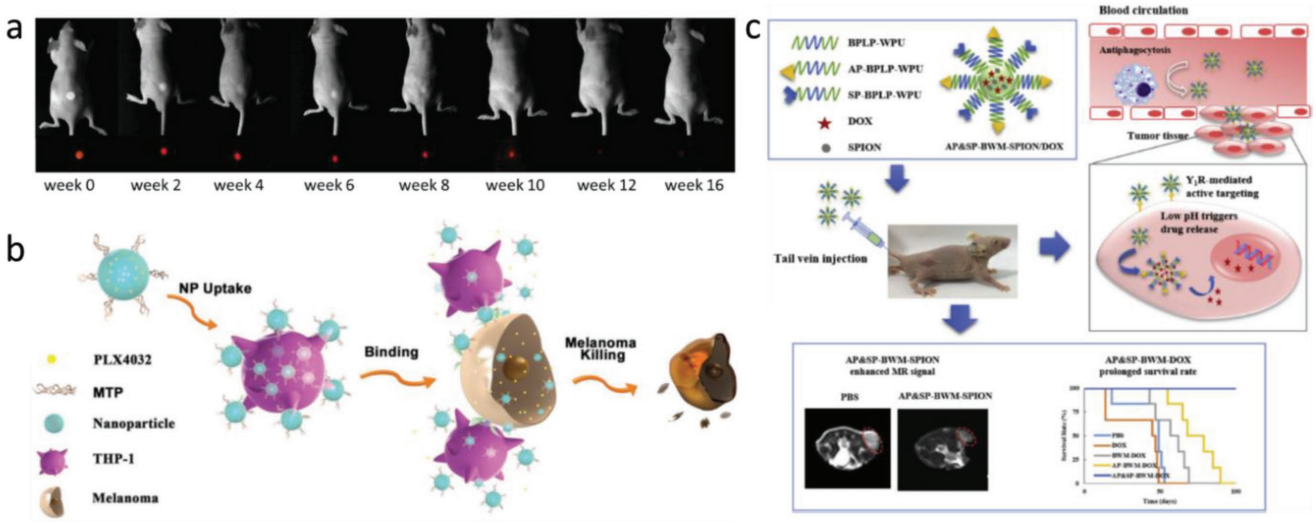

Figure 3. Biomedical applications of BPLPs. a) In vivo fluorescent images of BPLP-PLLA. Reproduced with permission.[35] Copyright 2014, Wiley-VCH. b) Schematic illustration of the immune cell-mediated nanoparticle delivery system targeting to cancer cells. Reproduced with permission.[53] Copyright 2016, Wiley-VCH. c) Schematic illustration of pH protective Y1 receptor ligand functionalized antiphagocytosis BPLP-WPU micelles for enhanced tumor imaging and therapy. Reproduced with permission.[51] Copyright 2018, Elsevier.

turned from a couple of months to over a year, while mainly relying on crosslinking conditions. After incorporating BPLP prepolymers with other biodegradable materials, such as polylactones, the degradation properties of the newly obtained fluorescent polymers were also studied.[33,35] As expected, the in vitro degradation rate strongly depended on the length of the incorporated hydrophobic polylactone blocks. For example, BPLP-Cys-PLLA20 (the molar ratio between BPLP-Cys prepolymer and LA monomers was 1:20) completely degraded after 12 weeks for PBS incubation, while the degradation rate of BPLP-Cys-PLLA100 (the molar ratio between BPLP-Cys prepolymer and LA monomers was 1:100) was similar to that of PLLA with correspondingly similar molecular weight. During the degradation process of citrate-based BPLPs, their fluorescence intensity also decayed accordingly and completely vanished at the end of the degradation, enabling noninvasive fluorescence imaging for tracking in vivo degradation of polymers.

3.2.2. Mechanical Properties

The mechanical properties of citrate-based BPLPs could also be turned by adjusting monomer ratios, crosslinking conditions, and chain extensions. Through changing monomer ratios (OD:CA:Cys 1:1:0.2/0.4/0.6/0.8), the crosslinked BPLP-Cys films exhibited tensile strength that ranged from 3.25 ± 0.13 to 6.5 ± 0.8 MPa and the initial modulus varied from 3.34 ± 0.15 to 7.02 ± 1.40 MPa. The films were elongated up to 240 ± 36%, which is comparable with the values for arteries and veins.[90] The compressive modulus of the BPLP-Cys (0.6) (OD:CA:Cys 1:1:0.6) scaffold was 39.60 ± 5.90 KPa, confirming the soft and elastic nature of the scaffolds.[31] After chain extension with urethane-doping, the crosslinked UBPLPs demonstrated soft and elastic, but strong mechanical properties. The crosslinked UBPLP films presented a tensile strength of 49.41 ± 6.17 MPa with a corresponding elongation of 334.87% ± 26.31%. Even the porous triphasic vascular scaffold made from crosslinked UBPLPs showed strong mechanical properties with a burst pressure of 769.33 ± 70.88 mmHg and a suture retention strength of 1.79 ± 0.11 N. With improved mechanical strength, UBPLPs offer great potential in the field of soft tissue engineering/drug delivery where bioimaging is also strongly desired.

3.2.3. Biocompatibility

To test the biocompatibility of citrate-based BPLPs, which were synthesized from natural or biocompatible monomers, both in vitro cytocompatibility and in vivo foreign body response studies were conducted.[31] The crosslinked BPLP-Cys films were found to support adhesion and proliferation of 3T3 fibroblast, and their degradation products showed a comparable cytocompatibility with PLGA75/25. When implanted in vivo, the crosslinked BPLP-Ser scaffolds did not cause noticeable edema and tissue necrosis on the tested animals. After implantation for 5 months, a thin fibrous capsule was produced, which was expected and common as a weak chronic inflammation introduced by foreign materials. Moreover, all modified BPLPs, including UBPLPs, BPLPLs, and ABPLPs, demonstrated favorable biocompatibility.[35,44,89] For instance, BPLP-Cys-PLLA nanoparticles presented lower cytotoxicity to 3T3 fibroblasts than BPLP-Cys prepolymer nanoparticles at high concentrations, and similar cytotoxicity to the widely used PLLA nanoparticles. In vivo animal studies on Sprague Dawley (SD) rats indicated that BPLP-Ser-PLLA generated comparable or even better tissue responses when compared to that of PLLA. Therefore, the biocompatibility of citrate-based BPLPs was proven by both in vitro and in vivo studies, offering them as great potential for various healthcare and regeneration applications.

3.3. Fluorescence Properties and Mechanisms of Citrate-Based BPLPs

3.3.1. Fluorescence Properties

After completing systematic studies on citrate-based BPLP prepolymers with all 20 natural (L-) α-amino acids, researchers found that all BPLP prepolymers had distinctive fluorescence, and their fluorescence properties were tunable by modifying the amino acids, monomer feeding ratio, and even excitation wavelengths for certain prepolymers.[31] Among all BPLP prepolymers, BPLP-Cys (using L-cysteine) prepolymer displayed the best fluorescence properties in terms of fluorescence intensity and QY. BPLP-Cys prepolymer exhibited a high QY of 62.3% and an excitation-independence fluorescence emission (≈430 nm). It also possessed a high photostability with photobleaching of about 2% after 3 h of continuous UV excitation, while the traditional organic dye rhodamine-B had about 10% photobleaching. BPLP-Ser (using L-serine), which had a QY of 26.0%, was the exemplified prepolymer that showed an excitation-dependence fluorescence emission after changing the excitation wavelength from 310 to 573 nm. The BPLP-Ser prepolymer could emit fluorescence from blue to red and even NIR by increasing excitation wavelengths. This unique property not only enables BPLP-Ser prepolymer to be a promising material for deep tissue NIR imaging, but also gives it potential as a candidate for multiplex imaging.

Due to the excellent fluorescence properties of BPLP-Cys and BPLP-Ser prepolymers, most chain extension studies were conducted on these two prepolymers, and fluorescence properties of newly developed fluorescent polymers were also investigated. In the study done by Yi et al.,[89] after the completion of urethane-doping, the QY of the resulting UBPLP-Cys (38.65%) and UBPLP-Ser (19.38%) had decreased when compared with their precursors of BPLP-Cys (62.3%) and BPLP-Ser (26.0%) prepolymers. However, the dependency between emission and excitation of the urethane-doped polymers were retained from their precursors, i.e., UBPLP-Cys had excitation-independent emission spectra, while UBPLP-Ser presented excitation-dependent emission spectra. Yang and co-workers also studied the fluorescence properties of BPLPLs,[33,35] and found that, generally, the fluorescence intensity and QY of BPLPLs were lower than that of BPLP prepolymers, and were decreased along with the ratios of introduced polylactones. BPLPL's dependency between emission and excitation also kept the inheritance of their prepolymer precursors.

3.3.2. Fluorescence Mechanisms

A handful of studies have been done to explore the fluorescence origin and mechanism of citrate-based BPLPs. Yang and co-workers discovered that the fluorescence of BPLPs was attributed to molecular fluorophores were formed by reacting CA and amine-containing molecules, while the diols providing no contribution.[31,32] A six-membered morphorline ring structure, having a structure similar to that of morpholine-2,5-dione, was initially hypothesized to be responsible for fluorescence. More recently, Yang and co-workers presented more systematic studies to showcase the fluorescence mechanism of CA derived fluorophores.[34] In these studies, a family of water-soluble fluorescent dyes, referred to as citric acid-derived photoluminescent dyes (CPDs) through facile one-pot reactions between CA and various amine-containing molecules such as amino acids, were synthesized. Two separate classes of CPDs, a thiozolopyridine family and a dioxopyridine family, were identified and their fluorescence mechanisms were studied by using computational modeling and time resolved fluorescence spectroscopy. The thiozolopyridine family of CPDs were reacted from equimolar amounts of citric acid and β-/γ-aminothiols, resulting in a two ring-fused thiazolo pyridine carboxylic acid (TPA) structure (which was in agreement with the report by Kasprzyk et al.[36]). Among the thiozolopyridine family, CA-Cys was a typical example, exhibiting strong fluorescence with a high QY of 81% and an extinction coefficient of 8640 M^{-1} cm^{-1}. CA-Cys also presented an excitation-independent fluorescence emission with a peak at ≈430 nm, in which the fluorescence usually resulted from the relaxation of the electronically excited singlet state in its lowest vibrational energy level to the ground state (Kasha's rule).[91] Similarly, strong excitation-independent fluorescence emissions were observed from other CPDs with TPA structures, including CA-homocysteine, CA-cysteamine, and CA-penicillamine. To further explore the fluorescence mechanism of TPA molecules, their aromaticity properties were calculated based on the Nucleus Independent Chemical Shift (NICS) model. All the TPA molecules demonstrated high aromaticity with NICS < −3.0, indicating the π–π^* electronic excitation that led to emission from the lowest energy band (similar to most organic with conjugated aromatic rings). The time-dependent fluorescence study demonstrated that CA-Cys had a single-exponential lifetime of $\tau = 9.86 \pm 0.078$ ns, which confirmed that the fluorescence emission of TPA molecules obeyed Kasha's rule (as illustrated by a Jablonski diagram). The second type of CPDs, dioxo-pyridine ring (DPR) structures, were prepared from reacting CA and amines lacking a thiol group, even including monofunctional amines such as heptylamine, whose fluorescence cannot be explained as a result of TPA. Unlike TPA molecules, DPR molecules showed relatively weak fluorescence with QYs lower than 40%, excitation-dependent emission (band shifting behavior), and dynamic Stokes shifts. The DPRs also had no conjugation structures, as supported by low aromaticity with NICS > 1.5. Therefore, the fluorescence mechanism of conventional conjugated organic dyes is not applicable for DPR molecules. The authors proposed that aliphatic tertiary nitrogen to be the source of fluorescence, which was subsequently confirmed by computational calculations. Specifically, n-π^* and n-σ^* transitions of the lone pair electrons of the tertiary amine undergo a red-shift of absorbance from a smaller HOMO–LUMO gap, which resulted from the electron withdrawing effects of the adjacent carbonyl groups. To further unveil the mechanism of the band shifting phenomenon of DPR molecules, time-resolved fluorescence spectroscopy was performed. Using CA-alanine (CA-Ala) as an example, a triple exponential model adequately fitted the lifetime decay, resulting in three individual lifetimes of $\tau_1 = 1.03 \pm 0.029$ ns, $\tau_2 = 4.33 \pm 0.128$ ns, and $\tau_3 = 10.07 \pm 0.031$ ns. The multiple lifetimes indicated that the band shifting phenomenon to be a result of the "red edge effect," where the presence of rotating

auxochromic groups generates additional dipole interactions between the fluorophore and solvent during intersystem relaxation, prolonging the solvation time to the approximate timescale of fluorescence emission,[92] and longer solvation time further relaxes the excited state to various lower energy levels, resulting in multiple lifetimes and red-shifting emissions. In addition, a correlation between the band shifting and solvent polarity further proved that the dynamic band shifting exhibited by DPR molecules was generated by the red-edge effect, which was ultimately governed by fluorophore/solvent interactions. Based on studies of the two types of CPDs, the authors summarized that the thiozolopyridine family generally presented high QY, long lifetime, and exceptional photostability, while the dioxopyridine family displayed relatively lower QY, multiple lifetimes, and solvent-dependent band shifting behavior. As such, a relatively comprehensive understanding of the fluorescence mechanisms of the fluorophores in citrate-based BPLPs was provided.

The high aromaticity of TPA molecules is responsible for their fluorescence properties, but may also cause the ACQ effect that limits their solid state applications, as demonstrated in the study by Chen et al.[93] The BPLPs successfully provide a polymer system enabling homogeneous dispersion of fluorescent TPA molecules to avoid their aggregation, which thereby obtain strong solid state fluorescence. DPR molecules have no conjugation structures, but also present decreased fluorescence at concentrated solutions. The reason of the decreased fluorescence might be partially attributed to inner filter effect, which means an apparent decrease in emission as a result of reabsorption of emitted radiation, although a more comprehensive mechanism is yet to be identified.

Opposite to the ACQ effect that happens on most traditional aromatic structures, a new phenomenon termed as ''aggregation induced emission'' (AIE) was discovered on a series of silole derivatives by Tang and co-workers in 2001.[94] These derivatives were not fluorescent in dilute solutions, but became highly luminescent when they were aggregated in concentrated solutions and solid state. Current mechanistic understanding concludes that there are two key factors that determine the AIE effect, one is the moieties have active intramolecular rotations/vibrations/motions that sufficiently dissipate excited-state energy in isolated states, and the other is twisted 3D structures in aggregate states to effectively prevent π–π stacking interactions. Up to now, many AIE systems that are termed as AIEgens have been developed.[95] For instance, tetraphenylethene (TPE) is a prototypical AIEgen comprising of a central olefin stator surrounded by four peripheral aromatic rotors (phenyl rings). In diluted solutions, the dynamic rotations of the aromatic rotors dissipate the exciton energy. Therefore, the solution is almost nonemissive. Upon aggregate formation, the emission of TPE is induced by the restricted intramolecular rotation (RIR) effect and the highly twisted 3D molecular conformation. In the past decade, a large amount of AIEgens have been applied for various applications including biological sensing and imaging probes, chemical sensing, optoelectronic systems, and stimuli responses. Moreover, in order to eliminate the undesirable ACQ effect that hinders solid applications of traditional aromatic systems (ACQphores), AIE elements have been integrated into ACQ systems to create ACQ-to-AIE transformations. For example, a prototypical AIEgen tetraphenylethene (TPE) has been used to decorate an ACQphore anthracene with three different ratios (2:1, 1:1, and 1:2). All groups exhibit a typical character of AIE effect. Due to the reactive nature of CA derived fluorophores and citrate-based CDs (discussed in Section 2), it is convenient to design citrate-based fluorescent biomaterials with ACQ-to-AIE transformation.

3.4. Biomedical Applications of Citrate-Based BPLPs

Due to their good biocompatibility, strong and tunable fluorescence performance, adjustable mechanical properties, as well as programmable degradation profiles, citrate-based BPLPs have great advantages in the fields of biological labeling and imaging, biosensing, drug delivery, and regenerative medicine. With the versatility in molecular design and fabrication, they have been fabricated into films, porous scaffolds, nanoparticles, micelles and nanogels for various applications.

Nanoparticles based on BPLP prepolymers, UBPLPs, and BPLPLs were easily fabricated by nanoprecipitation or single/double emulsion approaches.[31,89] By adding maleic acid into the chain of water soluble BPLPs, biodegradable and photoluminescent nanogels were created through photocrosslinking.[88] Stable nanosized micelles were also developed through self-assembly of ABPLPs[44] and BPLP-WPU.[51] These nanoparticles,[35] nanogels,[88] and micelles[44] all presented strong intrinsic fluorescence, and were successfully applied for cell labeling and in vivo fluorescence imaging. Moreover, they also provided the potential for drug delivery application. For example, UBPLP and BPLP-PLGA nanoparticles were used for 5-fluorouracil (5F) encapsulation and controlled release, and the encapsulation efficiency and release profiles were able to be regulated by using different preparation processes.[33,89] As a result of these advantages, citrate-based nanoparticles, nanogels, and micelles offer themselves as great candidates for performing theranostic nanomedicine without further incorporation of fluorescent components. By taking advantage of innate immune cells' ability to target tumor cells, Yang's lab developed a novel drug delivery system employing macrophages to carry and navigate BPLP-PLLA nanoparticles to achieve cancer specific drug delivery (Figure 3b).[53] Specifically, BPLP-PLLA nanoparticles encapsulated with an anti-BRAF V600E mutant melanoma specific drug (PLX4032) were first loaded to macrophage model cells, THP-1, through cell uptake. To improve the cell uptake efficiency of nanoparticles, the drug encapsulated BPLP-PLLA nanoparticles were modified with muramyl tripeptide (MTP). Later, guided by THP-1cells, the BPLP-PLLA nanoparticles, were delivered to melanoma cells, and the transported PLX4032 drugs was subsequently released to kill the cancer cells. Due to strong intrinsic photoluminescence of BPLP-PLLA nanoparticles, the high THP-1 uptake of nanoparticles and successful nanoparticle delivery were investigated by fluorescence imaging and flow cytometry. Pharmacological studies indicated that the novel drug delivery system effectively killed melanoma cells. Therefore, by taking advantage of the nature of interactions between immune cells and tumors, the immune cell-mediated nanoparticle targeting strategy enabled a "self-powered" drug delivery system, which provided

significant advancement in theranostic nanotechnologies for diseases involving immune responses.

As a response to the limitations, such as shallow penetration depth, of single modality fluorescence imaging technologies, multimodal imaging has drawn extensive attention due to its ability to provide more comprehensive spatial, temporal, structural, and high-resolution information.[96] Li et al. fabricated fluorescent nanobubbles (NBs) by encapsulating liquid tetradecafluorohexane (C6F14) with BPLP-Cys-PLLA, and then modified the NBs with PNBL-NPY ligand (a selective ligand of neuropeptide Y Y1 receptors (Y1Rs) overexpressed in breast tumors) for breast tumor targeting and imaging.[52] The PNBL-NPY modified NBs presented narrow size-distribution (polydispersity index (PDI) < 0.285) with averaged size value of 230.2 nm. In vitro and in vivo results indicated that the biocompatible NBs exhibit excellent fluorescence and ultrasound imaging capability and high specificity to Y1 receptor overexpressing breast cancer cells and tumors, providing a new nanoplatform for early cancer diagnosis and treatment. Wadajkar et al. developed fluorescence and magnetic resonance (MR) dual-imaging systems by utilizing oil soluble BPLP prepolymers to encapsulate magnetic nanoparticles (single emulsion method) or water soluble BPLP prepolymers to perform surface modification of magnetic nanoparticles (EDC/NHS chemistry).[45] In vitro prostate cells uptake studies indicated that successful optical and MR dual-imaging were performed by the resulting core–shell nanoparticles. Interestingly, different prostate cancer cells (PC3 and LNCaP cells) displayed selective uptake behaviors of the nanoparticles depending on hydrophilicity/hydrophobicity of particle surfaces. Recently, Jiang et al. synthetized Y1 receptor ligand [Asn6, Pro34]-NPY (AP) and self-peptide (SP) based BPLP-WPU polymeric micelles through self-assembling (Figure 3c).[51] AP is a pH sensitive and selective ligand of neuropeptide Y Y1 receptors (Y1Rs) overexpressed in breast tumors, which improves micelle stability during storage and blood circulation, but also increases tumor targeting and triggers drug release in the acidic tumor microenvironment. SP is able to reduce phagocytic clearance during blood circulation, minimizes the uptake of micelles in the liver and kidney, and further enhances micelle retention in the tumors. After loading superparamagnetic iron oxide nanoparticles (SPION), the micelles exhibited fluorescence and MR dual-imaging capabilities for cell and tumor imaging. Due to the excellent pH responsiveness, and tumor targeting efficiency and antiphagocytosis of the AP&SP comodified BPLP-WPU micelles, the doxorubicin (DOX) loaded micelles generated high therapeutic effect for breast tumors in vivo with prolonged survival time. This study may pave the way for safer and more specific Y1 receptor overexpressed breast cancer diagnosis and treatment.

Furthermore, with facile fabrication processes, including solvent evaporation, thermal crosslinking, and salt leaching, solid films and porous scaffolds have been prepared through crosslinked BPLPs, BPLPLs, and crosslinked UBPLPs, which all displayed strong fluorescence and favorable biocompatibility.[31,35,89] After subcutaneous implantation into animals, these films and scaffolds could be observed by noninvasive fluorescence imaging system. Thus, the citrate-based BPLPs could help patients and doctors to locate the implanted material, as well as monitor the degradation and performance simply by fluorescence imaging.

4. Citrate-Based Molecular Fluorophores

Due to the significant fluorescence properties of citrate-based molecule fluorophores that was demonstrated in the development of CDs and BPLPs, researchers have increased their efforts in developing new citrate-based fluorophores and expand their applications. In this section we will discuss current developments of the citrate-based molecular fluorophores.

4.1. Design and Preparation of Citrate-Based Molecular Fluorophores

Studies have indicated that the highest QY of citrate-based fluorescent materials are achieved using α,β-diamines, β-amino thiols and β-amino alcohols as precursors, which leads to the hypothesis that CA reacts with specific α,β-diamines, β-amino thiols, and β-amino alcohols to produce fluorescent organic molecular dyes.[37,97] To examine this hypothesis, Kasprzyk et al. reacted CA with five different bifunctional amines, including cysteamine, L-cysteine, *o*-aminophenol, *o*-aminothiophenol, and *o*-phenylenediamine, each at 180 °C for 1 h.[37] After being isolated with HPLC, their chemical structures were determined by ^{1}H, ^{13}C, and HSQC NMR experiments, elemental analysis, high resolution and fragmentation spectra ESI-MS analyses. The results indicated these fluorescent compounds consist of five-membered ring fused 2-pyridones. The obtained five molecular fluorophores all displayed strong absorption at around 260 and 350 nm, as a result of π–π^* transition of sp^2 carbons of aromatic and heterocyclic rings, and the n–π^* transition of C=O bonding, respectively. Their water solutions showed excitation-independent emission with maximum excitation wavelength at ≈350 nm and maximum emission wavelength in a range of 418–450 nm depending on the examined compound. They also exhibited high QYs above 60% with the highest QY of 79% achieved from reacting CA with *o*-aminophenol, which were comparable to those reported for organic fluorescent dyes such as rhodamines and coumarines (40–90%). The fluorescence decay curve suggested the fluorescence lifetimes of these molecules were in the range of 0.2–8.24 ns, which are common values for fluorescent organic dyes (<10 ns). Later, the authors developed additional molecular fluorophores by reacting CA with other α,β-bifunctional amines, including glutathione, *N*-methyloethylenediamine, 1,2-diaminopropane, and ethanolamine. All the characterizations proved the formation of specific five-membered ring fused 2-pyridone structures in the above synthesized organic compounds. Furthermore, the authors developed fluorescent molecular compounds by reacting CA with α,γ-bifunctional amines, such as 1,3-diaminopropane, 3-amino-1-propanol. The resulting fluorescent molecules were confirmed with six-membered ring fused 2-pyridone structures and molecular composition of $C_9H_{10}N_2O_3$ and $C_9H_{10}NO_4$, respectively. Yang and co-workers also prepared a series of CA based fluorophores via heating CA with various primary amines, amino acids, or analogs of amino acids.[34] After

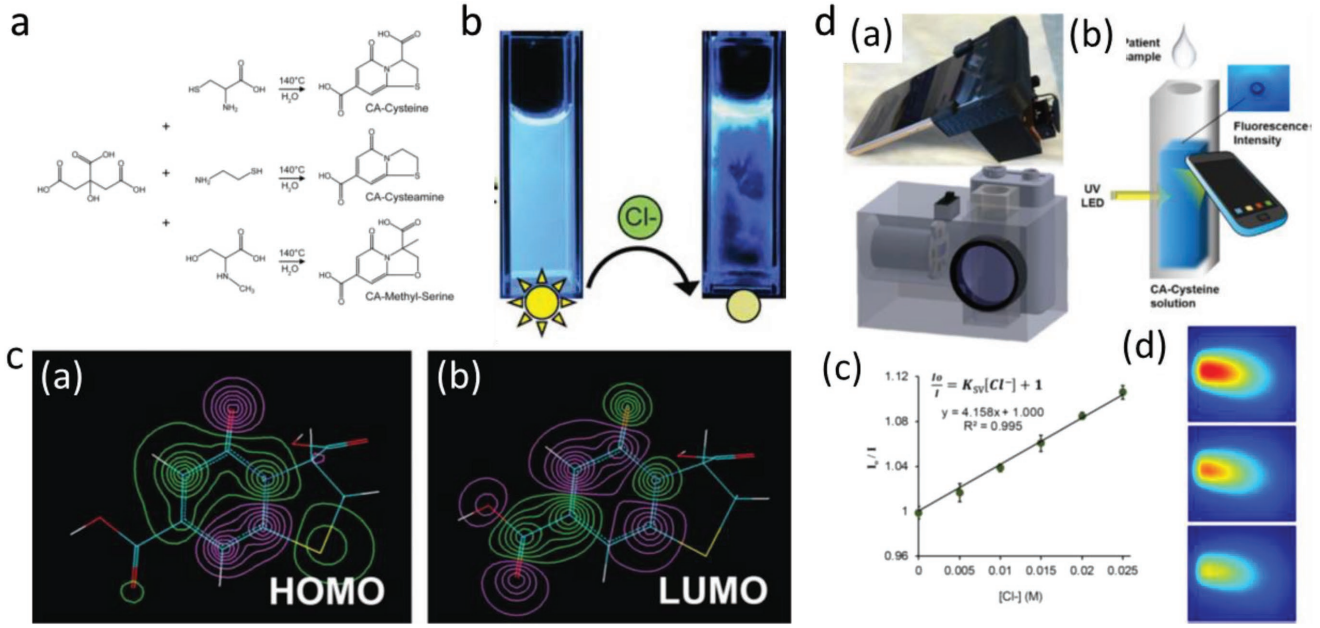

Figure 4. Biomedical applications of citrate based molecular fluorophores. a) Facile synthesis scheme of citric acid and various primary. b) Chloride detection from quenching of CA-Cys fluorescence intensity. c) (ca) HOMO and (cb) LUMO isosurface plots highlight planarity and an aromatic 2-pyridone element responsible for the bright fluorescence of CA-Cys. Reproduced with permission.[50] Copyright 2017, the Royal Society of Chemistry. d) The smartphone-based chloridometer for point-of-care diagnostics of cystic fibrosis. Reproduced with permission.[55] Copyright 2017, Elsevier.

analyses of chemical structures and fluorescence properties, fluorescence mechanism based on TPA and DPR structures were established, depending on the choices of amines. As such, the authors proposed several amine reagents which can readily be used to prepare efficient CA based fluorescent molecules.

4.2. Biomedical Applications of Citrate-Based Molecular Fluorophores

4.2.1. Biosensing

With a better understanding of the structures and fluorescence mechanisms of CA based fluorophores, corresponding applications have recently been developed. For example, Fang et al. experimented with TPA molecule for free chlorine sensing.[98] Specifically, the TPA molecule (CA-Cys) was synthesized from the condensation of CA and L-cysteine, and the obtained TPA molecule exhibited strong blue fluorescence (QY 90.5%) with a maximum excitation at 345 nm and a maximum emission at 415 nm. It was found that the fluorescence signal of TPA can be quenched sensitively by the free chlorine, which was determined by the oxidation of sulfur atom of TPA into sulfoxide chlorine. By adjusting pH values, a maximum quenching efficiency occurred pH 4. The detection limit was calculated to be about 0.2×10^{-6} M, which is sufficient to meet the requirement for free chlorine concentration range (0.05–5 mg L^{-1} (1.4–140) $\times 10^{-6}$ M) in most water samples. If necessary, the detection limit of the sensor can be tuned by adjusting the concentration of TPA. For instance, a 0.3×10^{-6} M TPA solution would reach a detection limit of 8×10^{-9} M of free chlorine. The developed sensor was also applied for detecting the concentration of free chlorine in a local tap water sample. The free chlorine concentration measured by the newly developed sensor [$(6.11 \pm 0.05) \times 10^{-6}$ M] consistent with that obtained from the most popular colorimetry method based on *N*,*N*-diethyl-*p*-phenylenediamine (DPD) ($(6.06 \pm 0.17) \times 10^{-6}$ M). Based on the results mentioned above, the authors further developed a visible PL ratiometric sensor using $Ru(bpy)_3Cl_2 \cdot 6H_2O$ as a red background fluorescence signal, which provided a convenient method for the on-site and on-line detection of free chlorine. Kim et al. also developed a class of fluorescence chloride sensors based on CA derived fluorophores, utilizing dynamic quenching mechanisms (**Figure 4**a–c).[50] In detail, a family of citrate-based fluorophores for chloride sensing were synthesized via a simple one-pot reaction of CA and a primary amine (L-cysteine, cysteamine, or methyl serine) in water. Taking CA-Cysteine (CA-Cys), which presented strong fluorescence with a high QY of 81% and a long lifetime of 10.06 ns, as an example, it is generally insensitive to chloride, but dynamic quenching by both protons and chloride happens when pH was below 2.4. These quenching behaviors were translated into a practical sensing method by linearizing the quenching effects of two dynamic quenchers (protons and chloride) according to the modified Stern–Volmer (SV) equation, and each SV plot of quenching rate versus quencher concentration produces a slope that is linear for dynamic quenchers, then the chloride sensitivity from the slope of each standard curve at selected pH levels could be obtained, from which an unknown chloride sample would be analyzed under the same dye strength and acidity. The authors also demonstrated the clinical utility of citrate-based sensors as a sweat chloride test method for the diagnosis of CF. The clinical performance of CA-Cys was compared to standard mercuric nitrate titration for the determination of

sweat chloride from 13 individuals with/without CF, resulting an intraclass correlation coefficient (ICC) of 0.984 with a 95% confidence interval of (0.948, 0.995). In addition, molecular modeling studies demonstrated the structural mechanism behind chloride sensing, expanding the citrate-based fluorescence sensors with improved chloride sensitivities. Moreover, the authors demonstrated the multihalide sensing ability of developed citrate-based sensors. Therefore, citrate-based fluorescent molecular compounds have potential to enable low-cost, automated multianalysis systems for simpler, yet accurate, point-of-care clinical diagnostics. As a next step, the authors designed a smartphone operated chloridometer that aimed to optimizes the analytical performance of the citrate-based sensing materials for the detection of chloride in sweat (Figure 4d).[55] The chloridometer was equipped with an ultraviolet (UV) light emitting diode (LED) light source to generate fluorescence from the citrate-based sensor, which was then collected and measured by the smartphone camera for quantitative determination of chloride from prepared samples. The sensor exhibited a wide linear range of (0.8–200) $\times 10^{-3}$ M chloride (relative standard deviations below 1%). Clinical validation was also performed by the smartphone operated chloridometer with sweat from individuals with/without CF, demonstrating convenient sweat diagnostics with reliable detection of CF. The newly developed chloride sensing device may have broad impact on the realization of diagnostic tests in resource-scarce settings with limited access to sophisticated instrumentation.

4.2.2. Material Fluorescence Functionalization

In addition, citrate-based molecular fluorophores could be used to functionalize different materials with fluorescence properties. For example, researchers revealed the reaction possibility of citrate-based molecular fluorophores by reacting TPA (CA-Cys) and DPR (CA-Ala) structured fluorophores with 1,8-octanediol.[34,36] LC–ESI–MS mass spectrum confirmed the ester bonds between fluorophores and diols. Fluorescence studies also showed that the resulting BPLP-TPA had identical fluorescence properties as that of CA-Cys and BPLP-Cys, including an excitation-independent emission. The BPLP-DPR also presented a similar fluorescence property as CA-Ala which had an excitation-dependent emission. Furthermore, Kasprzyk et al. incorporated fluorescent derivative of 2-pyridone into silicone matrix via condensation of citric acid with α,β-diamine groups through a two-step approach.[99] In the first step, α,β-diamine moieties (*N*-[3-(trimethoxysilyl)propyl] ethylenediamine (TMS)) was chemically incorporated into silicone polymer. The second step involved surface condensation of these α,β-diamine groups with CA. The resulting fluorescent molecules constituted of 2-pyridone structure referred to as 5-oxo-1,2,3,5-tetrahydroimidazo[1,2-*a*]pyridine-7-carboxylic acid (the same as IPCA that name by Song et al.[27]). The citrate-based fluorophore modified silicone material was further exploited for sensing of iron ions, chromates and ascorbic acid. Recently, CA-Cys fluorophores were also used to modify cellulose by simply soaking cellulose in a concentrated CA/cysteine aqueous solution followed by drying above 80 °C.[93] The chemical conjugation occurred and increased with drying temperature (with a highest conjugating ratio of 1.6 wt%). The conjugation of CA-Cys had no effect on the crystallinity structural properties of the cellulose, but introduced remarkable fluorescence, exhibiting an excitation-independent emission (435 nm) under excitation at 360 nm, to the material system. Under UV light (365 nm) irradiation, the modified cellulose powders displayed a significantly brighter blue emission when compared to that of pure CA-Cys, suggesting that cellulose was responsible for providing the chemical basis for CA-Cys to avoid its solid-state quenching. In addition, researchers confirmed the potential applications of the modified cellulose, such as anticounterfeiting, chloride sensing, and UV shielding.

4.2.3. Molecular and Cellular Labeling

To demonstrate the potential of citrate-based molecular fluorophores for molecular and cellular labeling, Yang and co-workers first conjugated the fluorophores with bovine serum albumin (BSA) and fibroblast cells.[34] The molecular/cellular labeling were achieved through conjugation between free carboxyl groups of molecular fluorophores and the surface of BSA/fibroblasts using carbodiimide chemistry. Strong blue fluorescence emission was observed from BSA molecules conjugated with CA-Cys, which indicated the molecular labeling capability of CA-Cys fluorophores. Moreover, CA-Ala molecules with activated carboxyl groups were used for fibroblasts labeling. Due to the band shifting behavior of CA-Ala fluorophores, the fibroblast cells labeled with CA-Ala exhibited strong green fluorescence in the FITC channel of confocal microscopy, indicating the great potential of molecular fluorophores for cellular labeling and visualization.

5. Conclusion

In this review, we summarized the family of citrate-based fluorescent biomaterials, including citrate-based CDs, citrate-based BPLPs, and citrate-based small molecular fluorophores. Their design and synthesis strategies, materials properties, fluorescence performances, and mechanisms, and relevant biomedical applications (e.g., bioimaging, biosensing, and biomedicine) were systematically discussed. All categories of citrate-based fluorescent biomaterials demonstrated favorable biocompatibility, easy synthesis, versatile designability, as well as strong fluorescence with high QY and tunable excitation/emission wavelengths (from blue to NIR), leading to versatile functionalities in theranostic healthcare and regenerative engineering. Despite the significant progresses mentioned above, further explorations on citrate-based fluorescent biomaterials are demanded, as our current understanding of the structures and components of citrate-based fluorescent biomaterials remains inadequate, hindering the full knowledge of their fluorescence origins and mechanisms. More advanced techniques and analyses are needed to gain a more comprehensive understanding and better regulation of material properties. In addition, the citrate-based fluorescent biomaterials may also be suitable for multimodality imaging that could deliver more comprehensive information by combining with imaging techniques such as MRI, ultrasound imaging, and photoacoustic (PA) imaging. In the future, even more complicated fluorescence techniques,

such as fluorescence resonance energy transfer (FRET), aggregation-induced emission (AIE), and multiphoton induced fluorescence, may be realized and introduced to the citrate-based fluorescent biomaterial systems. Due to their noninvasive real-time imaging capability, the citrate-based fluorescent biomaterials would be applied for monitoring in vivo scaffold degradation and tissue infiltration/formation, which had been a prevailing challenge in the evolving field of tissue engineering. Finally, citrate-based biomaterials can be endowed with versatile functionalities through interactions with different functional components (growth factors, drugs, antibodies, etc.), biomaterials, and even cells for more medical applications.

Acknowledgements

The authors would like to acknowledge financial support from the National Institutes of Health Awards (CA182670, EB024829, and AR072731), a Cystic Fibrosis Foundation Research Award (Yang17G0), and a National Natural Science Foundation of China Award (31529002). The authors also thank Mr. Digeng Du for editing assistance.

Conflict of Interest

J.Y. and The Pennsylvania State University have a financial interest in Acuitive Technologies, Inc. These interests have been reviewed by the University's Institutional and Individual Conflict of Interest Committees and are currently being managed by the University.

Keywords

bioimaging, carbon dots, citric acid, degradation, fluorescence

Received: May 15, 2018
Revised: June 29, 2018
Published online: July 26, 2018

[1] A. A. Appel, M. A. Anastasio, J. C. Larson, E. M. Brey, *Biomaterials* **2013**, *34*, 6615.
[2] a) N. Artzi, N. Oliva, C. Puron, S. Shitreet, S. Artzi, A. bon Ramos, A. Groothuis, G. Sahagian, E. R. Edelman, *Nat. Mater.* **2011**, *10*, 704; b) J. H. Park, L. Gu, G. von Maltzahn, E. Ruoslahti, S. N. Bhatia, M. J. Sailor, *Nat. Mater.* **2009**, *8*, 331; c) O. S. Wolfbeis, *Chem. Soc. Rev.* **2015**, *44*, 4743.
[3] a) C. Zheng, M. Zheng, P. Gong, D. Jia, P. Zhang, B. Shi, Z. Sheng, Y. Ma, L. Cai, *Biomaterials* **2012**, *33*, 5603; b) Z. Guo, S. Park, J. Yoon, I. Shin, *Chem. Soc. Rev.* **2014**, *43*, 16; c) S. A. Hilderbrand, R. Weissleder, *Curr. Opin. Chem. Biol.* **2010**, *14*, 71.
[4] F. Wang, W. B. Tan, Y. Zhang, X. Fan, M. Wang, *Nanotechnology* **2006**, *17*, R1.
[5] U. Resch-Genger, M. Grabolle, S. Cavaliere-Jaricot, R. Nitschke, T. Nann, *Nat. Methods* **2008**, *5*, 763.
[6] a) X. Cheng, E. Hinde, D. M. Owen, S. B. Lowe, P. J. Reece, K. Gaus, J. J. Gooding, *Adv. Mater.* **2015**, *27*, 6144; b) S. Xu, D. Li, P. Wu, *Adv. Funct. Mater.* **2015**, *25*, 1127; c) P. Zrazhevskiy, M. Sena, X. Gao, *Chem. Soc. Rev.* **2010**, *39*, 4326.
[7] B. A. Kairdolf, A. M. Smith, T. H. Stokes, M. D. Wang, A. N. Young, S. Nie, *Annu. Rev. Anal. Chem.* **2013**, *6*, 143.
[8] N. C. Shaner, P. A. Steinbach, R. Y. Tsien, *Nat. Methods* **2005**, *2*, 905.
[9] W. J. Sell, T. H. Easterfield, *J. Chem. Soc., Trans.* **1893**, *63*, 1035.
[10] U. Olthoff, R. Hüttenrauch, K. Matthey, *Tetrahedron* **1971**, *27*, 3447.
[11] T. K. Masatake Hori, Hayao Ueno, Hiroshi Morimoto, *Biochem. Med.* **1974**, *11*, 11.
[12] X. Xu, R. Ray, Y. Gu, H. J. Ploehn, L. Gearheart, K. Raker, W. A. Scrivens, *J. Am. Chem. Soc.* **2004**, *126*, 2.
[13] a) S. Y. Lim, W. Shen, Z. Gao, *Chem. Soc. Rev.* **2015**, *44*, 362; b) R. Wang, K. Q. Lu, Z. R. Tang, Y. J. Xu, *J. Mater. Chem. A* **2017**, *5*, 3717; c) F. Yuan, S. Li, Z. Fan, X. Meng, L. Fan, S. Yang, *Nano Today* **2016**, *11*, 565; d) J. Zhang, S. H. Yu, *Mater. Today* **2016**, *19*, 382.
[14] P. Namdari, B. Negahdari, A. Eatemadi, *Biomed. Pharmacother.* **2017**, *87*, 209.
[15] S. Tao, S. Zhu, T. Feng, C. Xia, Y. Song, B. Yang, *Mater. Today Chem.* **2017**, *6*, 13.
[16] Y. Wang, A. Hu, *J. Mater. Chem. C* **2014**, *2*, 6921.
[17] Q. Ye, F. Yan, Y. Luo, Y. Wang, X. Zhou, L. Chen, *Spectrochim. Acta, A* **2017**, *173*, 854.
[18] Y. Dong, H. Pang, H. B. Yang, C. Guo, J. Shao, Y. Chi, C. M. Li, T. Yu, *Angew. Chem., Int. Ed. Engl.* **2013**, *52*, 7800.
[19] X. Miao, D. Qu, D. Yang, B. Nie, Y. Zhao, H. Fan, Z. Sun, *Adv. Mater.* **2018**, *30*, 1704740.
[20] S. Qu, X. Liu, X. Guo, M. Chu, L. Zhang, D. Shen, *Adv. Funct. Mater.* **2014**, *24*, 2689.
[21] S. Qu, X. Wang, Q. Lu, X. Liu, L. Wang, *Angew. Chem., Int. Ed. Engl.* **2012**, *51*, 12215.
[22] Y. Dong, J. Shao, C. Chen, H. Li, R. Wang, Y. Chi, X. Lin, G. Chen, *Carbon* **2012**, *50*, 4738.
[23] N. Dhenadhayalan, K. C. Lin, R. Suresh, P. Ramamurthy, *J. Phys. Chem. C* **2016**, *120*, 1252.
[24] M. J. Krysmann, A. Kelarakis, P. Dallas, E. P. Giannelis, *J. Am. Chem. Soc.* **2012**, *134*, 747.
[25] J. Schneider, C. J. Reckmeier, Y. Xiong, M. von Seckendorff, A. S. Susha, P. Kasák, A. L. Rogach, *J. Phys. Chem. C* **2017**, *121*, 2014.
[26] A. Sharma, T. Gadly, S. Neogy, S. K. Ghosh, M. Kumbhakar, *J. Phys. Chem. Lett.* **2017**, *8*, 1044.
[27] Y. Song, S. Zhu, S. Zhang, Y. Fu, L. Wang, X. Zhao, B. Yang, *J. Mater. Chem. C* **2015**, *3*, 5976.
[28] S. Zhu, X. Zhao, Y. Song, S. Lu, B. Yang, *Nano Today* **2016**, *11*, 128.
[29] a) J. Guo, G. B. Kim, D. Shan, J. P. Kim, J. Hu, W. Wang, F. G. Hamad, G. Qian, E. B. Rizk, J. Yang, *Biomaterials* **2017**, *112*, 275; b) J. Guo, W. Wang, J. Hu, D. Xie, E. Gerhard, M. Nisic, D. Shan, G. Qian, S. Zheng, J. Yang, *Biomaterials* **2016**, *85*, 204; c) J. Guo, Z. Xie, R. T. Tran, D. Xie, D. Jin, X. Bai, J. Yang, *Adv. Mater.* **2014**, *26*, 1906; d) C. Ma, E. Gerhard, Q. Lin, S. Xia, A. D. Armstrong, J. Yang, *Bioact. Mater.* **2018**, *3*, 19; e) M. Mehdizadeh, H. Weng, D. Gyawali, L. Tang, J. Yang, *Biomaterials* **2012**, *33*, 7972; f) R. T. Tran, W. M. Choy, H. Cao, I. Qattan, J. C. Chiao, W. Y. Ip, K. W. Yeung, J. Yang, *J. Biomed. Mater. Res. A* **2014**, *102*, 2793; g) D. Xie, J. Guo, M. Mehdizadeh, R. T. Tran, R. Chen, D. Sun, G. Qian, D. Jin, X. Bai, J. Yang, *J. Mater. Chem. B* **2015**, *3*, 387; h) D. Shan, C. Zhang, S. Kalaba, N. Mehta, G. B. Kim, Z. Liu, J. Yang, *Biomaterials* **2017**, *143*, 142.
[30] R. T. Tran, J. Yang, G. A. Ameer, *Annu. Rev. Mater. Res.* **2015**, *45*, 277.
[31] J. Yang, Y. Zhang, S. Gutam, L. Liu, J. Dey, W. Chen, R. P. Mason, C. A. Serrano, K. A. Schug, L. Tang, *Proc. Natl. Acad. Sci. USA* **2009**, *106*, 10086
[32] Y. Zhang, J. Yang, *J. Mater. Chem. B* **2013**, *1*, 132.
[33] J. Hu, J. Guo, Z. Xie, D. Shan, E. Gerhard, G. Qian, J. Yang, *Acta. Biomater.* **2016**, *29*, 307.
[34] Z. Xie, J. P. Kim, Q. Cai, Y. Zhang, J. Guo, R. S. Dhami, L. Li, B. Kong, Y. Su, K. A. Schug, J. Yang, *Acta. Biomater.* **2017**, *50*, 361.
[35] Z. Xie, Y. Zhang, L. Liu, H. Weng, R. P. Mason, L. Tang, K. T. Nguyen, J. T. Hsieh, J. Yang, *Adv. Mater.* **2014**, *26*, 4491.
[36] W. Kasprzyk, S. Bednarz, D. Bogdal, *Chem. Commun.* **2013**, *49*, 6445.

[37] W. Kasprzyk, S. Bednarz, P. Żnudzki, M. Galica, D. Bogdał, *RSC Adv.* **2015**, *5*, 34795.
[38] L. Shi, J. H. Yang, H. B. Zeng, Y. M. Chen, S. C. Yang, C. Wu, H. Zeng, O. Yoshihito, Q. Zhang, *Nanoscale* **2016**, *8*, 14374.
[39] A. Iqbal, K. Iqbal, L. Xu, B. Li, D. Gong, X. Liu, Y. Guo, W. Liu, W. Qin, H. Guo, *Sens. Actuators, B* **2018**, *255*, 1130.
[40] K. Jiang, S. Sun, L. Zhang, Y. Lu, A. Wu, C. Cai, H. Lin, *Angew. Chem., Int. Ed. Engl.* **2015**, *54*, 5360.
[41] D. Wang, Z. Wang, Q. Zhan, Y. Pu, J.-X. Wang, N. R. Foster, L. Dai, *Engineering* **2017**, *3*, 402.
[42] W. Yang, H. Zhang, J. Lai, X. Peng, Y. Hu, W. Gu, L. Ye, *Carbon* **2018**, *128*, 78.
[43] S. Zhu, Q. Meng, L. Wang, J. Zhang, Y. Song, H. Jin, K. Zhang, H. Sun, H. Wang, B. Yang, *Angew. Chem., Int. Ed. Engl.* **2013**, *52*, 3953.
[44] D. Gyawali, S. Zhou, R. T. Tran, Y. Zhang, C. Liu, X. Bai, J. Yang, *Adv. Healthcare Mater.* **2014**, *3*, 182.
[45] A. S. Wadajkar, T. Kadapure, Y. Zhang, W. Cui, K. T. Nguyen, J. Yang, *Adv. Healthcare Mater.* **2012**, *1*, 450.
[46] Y. Ding, J. Ling, J. Cai, S. Wang, X. Li, M. Yang, L. Zha, J. Yan, *Anal. Methods* **2016**, *8*, 1157.
[47] Y. Wang, S. H. Kim, L. Feng, *Anal. Chim. Acta* **2015**, *890*, 134.
[48] Q. Zhang, C. Zhang, Z. Li, J. Ge, C. Li, C. Dong, S. Shuang, *RSC Adv.* **2015**, *5*, 95054.
[49] M. Zheng, Z. Xie, D. Qu, D. Li, P. Du, X. Jing, Z. Sun, *ACS Appl. Mater. Interfaces* **2013**, *5*, 13242.
[50] J. P. Kim, Z. Xie, M. Creer, Z. Liu, J. Yang, *Chem. Sci.* **2017**, *8*, 550.
[51] Z. Jiang, Y. Tian, D. Shan, Y. Wang, E. Gerhard, J. Xia, R. Huang, Y. He, A. Li, J. Tang, H. Ruan, Y. Li, J. Li, J. Yang, A. Wu, *Biomaterials* **2018**, *170*, 70.
[52] J. Li, Y. Tian, D. Shan, A. Gong, L. Zeng, W. Ren, L. Xiang, E. Gerhard, J. Zhao, J. Yang, A. Wu, *Biomaterials* **2017**, *116*, 106.
[53] Z. Xie, Y. Su, G. B. Kim, E. Selvi, C. Ma, V. Aragon-Sanabria, J. T. Hsieh, C. Dong, J. Yang, *Small* **2017**, *13*, 1603121.
[54] D. Li, P. Jing, L. Sun, Y. An, X. Shan, X. Lu, D. Zhou, D. Han, D. Shen, Y. Zhai, S. Qu, R. Zboril, A. L. Rogach, *Adv. Mater.* **2018**, *30*, 1705913.
[55] C. Zhang, J. P. Kim, M. Creer, J. Yang, Z. Liu, *Biosens. Bioelectron.* **2017**, *97*, 164.
[56] H. Li, Z. Kang, Y. Liu, S.-T. Lee, *J. Mater. Chem.* **2012**, *22*, 24230.
[57] X. Hu, L. Cheng, N. Wang, L. Sun, W. Wang, W. Liu, *RSC Adv.* **2014**, *4*, 18818.
[58] F. Wang, Z. Xie, H. Zhang, C.-y. Liu, Y.-g. Zhang, *Adv. Funct. Mater.* **2011**, *21*, 1027.
[59] X. Zhai, P. Zhang, C. Liu, T. Bai, W. Li, L. Dai, W. Liu, *Chem. Commun.* **2012**, *48*, 7955.
[60] M. L. Bhaisare, A. Talib, M. S. Khan, S. Pandey, H. F. Wu, *Microchim. Acta* **2015**, *182*, 2173.
[61] a) F. Gao, S. Ma, J. Li, K. Dai, X. Xiao, D. Zhao, W. Gong, *Carbon* **2017**, *112*, 131; b) J. Zhang, L. Yang, Y. Yuan, J. Jiang, S. H. Yu, *Chem. Mater.* **2016**, *28*, 4367.
[62] Z. Tian, X. Zhang, D. Li, D. Zhou, P. Jing, D. Shen, S. Qu, R. Zboril, A. L. Rogach, *Adv. Opt. Mater.* **2017**, *5*, 1700416.
[63] L. Deng, X. Wang, Y. Kuang, C. Wang, L. Luo, F. Wang, X. Sun, *Nano Res.* **2015**, *8*, 2810.
[64] E. J. Goh, K. S. Kim, Y. R. Kim, H. S. Jung, S. Beack, W. H. Kong, G. Scarcelli, S. H. Yun, S. K. Hahn, *Biomacromolecules* **2012**, *13*, 2554.
[65] M. Zheng, S. Liu, J. Li, D. Qu, H. Zhao, X. Guan, X. Hu, Z. Xie, X. Jing, Z. Sun, *Adv. Mater.* **2014**, *26*, 3554.
[66] L. Pan, S. Sun, A. Zhang, K. Jiang, L. Zhang, C. Dong, Q. Huang, A. Wu, H. Lin, *Adv. Mater.* **2015**, *27*, 7782.
[67] D. Qu, M. Zheng, L. Zhang, H. Zhao, Z. Xie, X. Jing, R. E. Haddad, H. Fan, Z. Sun, *Sci. Rep.* **2014**, *4*, 5294.
[68] S. Qu, D. Zhou, D. Li, W. Ji, P. Jing, D. Han, L. Liu, H. Zeng, D. Shen, *Adv. Mater.* **2016**, *28*, 3516.
[69] S. Sun, L. Zhang, K. Jiang, A. Wu, H. Lin, *Chem. Mater.* **2016**, *28*, 8659.
[70] a) S. N. Baker, G. A. Baker, *Angew. Chem., Int. Ed. Engl.* **2010**, *49*, 6726; b) F. Zu, F. Yan, Z. Bai, J. Xu, Y. Wang, Y. Huang, X. Zhou, *Microchim. Acta* **2017**, *184*, 1899.
[71] M. Hassan, V. G. Gomes, A. Dehghani, S. M. Ardekani, *Nano Res.* **2017**, *11*, 1.
[72] R. Ye, C. Xiang, J. Lin, Z. Peng, K. Huang, Z. Yan, N. P. Cook, E. L. Samuel, C. C. Hwang, G. Ruan, G. Ceriotti, A. R. Raji, A. A. Marti, J. M. Tour, *Nat. Commun.* **2013**, *4*, 2943.
[73] R. J. Robertson, G. A. J. Amaratunga, *J. Appl. Phys.* **1996**, *80*, 2998.
[74] Y. Dong, J. Cai, X. You, Y. Chi, *Analyst* **2015**, *140*, 7468.
[75] G. Eda, Y. Y. Lin, C. Mattevi, H. Yamaguchi, H. A. Chen, I. S. Chen, C. W. Chen, M. Chhowalla, *Adv. Mater.* **2010**, *22*, 505.
[76] a) F. Yuan, Z. Wang, X. Li, Y. Li, Z. Tan, L. Fan, S. Yang, *Adv. Mater.* **2017**, *29*, 1604436; b) J. Tang, B. Kong, H. Wu, M. Xu, Y. Wang, Y. Wang, D. Zhao, G. Zheng, *Adv. Mater.* **2013**, *25*, 6569.
[77] M. Fu, F. Ehrat, Y. Wang, K. Z. Milowska, C. Reckmeier, A. L. Rogach, J. K. Stolarczyk, A. S. Urban, J. Feldmann, *Nano Lett.* **2015**, *15*, 6030.
[78] M. Sun, S. Qu, Z. Hao, W. Ji, P. Jing, H. Zhang, L. Zhang, J. Zhao, D. Shen, *Nanoscale* **2014**, *6*, 13076.
[79] J. Zheng, Y. Wang, F. Zhang, Y. Yang, X. Liu, K. Guo, H. Wang, B. Xu, *J. Mater. Chem. C* **2017**, *5*, 8105.
[80] J. Chen, J. Liu, J. Li, L. Xu, Y. Qiao, *J. Colloid. Interface Sci.* **2017**, *485*, 167.
[81] Y. Wang, D. Gao, Y. Chen, G. Hu, H. Liu, Y. Jiang, *RSC Adv.* **2016**, *6*, 79043.
[82] N. M. Zholobak, A. L. Popov, A. B. Shcherbakov, N. R. Popova, M. M. Guzyk, V. P. Antonovich, A. V. Yegorova, Y. V. Scrypynets, LeonenkoII , A. Y. Baranchikov, V. K. Ivanov, *Beilstein J. Nanotechnol.* **2016**, *7*, 1905.
[83] Z. Zhang, J. Chen, Y. Duan, W. Liu, D. Li, Z. Yan, K. Yang, *Luminescence* **2018**, *33*, 318.
[84] a) L. Qiao, S. Qian, Y. Wang, S. Yan, H. Lin, *Chemistry* **2018**, *24*, 4703; b) S. Sun, K. Jiang, S. Qian, Y. Wang, H. Lin, *Anal. Chem.* **2017**, *89*, 5542.
[85] S. M. Janib, A. S. Moses, J. A. MacKay, *Adv. Drug Delivery Rev.* **2010**, *62*, 1052.
[86] L. Yuan, W. Lin, K. Zheng, L. He, W. Huang, *Chem. Soc. Rev.* **2013**, *42*, 622.
[87] a) J. Yu, C. Wu, X. Zhang, F. Ye, M. E. Gallina, Y. Rong, I. C. Wu, W. Sun, Y. H. Chan, D. T. Chiu, *Adv. Mater.* **2012**, *24*, 3498; b) F. Song, W. C. Chan, *Nanotechnology* **2011**, *22*, 494006.
[88] D. Gyawali, J. P. Kim, J. Yang, *Bioact. Mater.* **2018**, *3*, 39.
[89] Y. Zhang, R. T. Tran, I. S. Qattan, Y. T. Tsai, L. Tang, C. Liu, J. Yang, *Biomaterials* **2013**, *34*, 4048.
[90] J. Yang, A. R. Webb, G. A. Ameer, *Adv. Mater.* **2004**, *16*, 511.
[91] A. N. Fletcher, *J. Phys. Chem.* **1968**, *72*, 8.
[92] A. P. Demchenko, *Luminescence* **2002**, *17*, 19.
[93] H. Chen, X. Yan, Q. Feng, P. Zhao, X. Xu, D. H. L. Ng, L. Bian, *ACS. Sustainable Chem. Eng.* **2017**, *5*, 11387.
[94] J. Luo, Z. Xie, J. W. Y. Lam, L. Cheng, B. Z. Tang, H. Chen, C. Qiu, H. S. Kwok, X. Zhan, Y. Liu, D. Zhu, *Chem. Commun.* **2001**, 1740.
[95] a) Y. Hong, J. W. Lam, B. Z. Tang, *Chem. Commun.* **2009**, 4332; b) J. Mei, Y. Hong, J. W. Lam, A. Qin, Y. Tang, B. Z. Tang, *Adv. Mater.* **2014**, *26*, 5429; c) J. Mei, N. L. Leung, R. T. Kwok, J. W. Lam, B. Z. Tang, *Chem. Rev.* **2015**, *115*, 11718.
[96] a) L. Cheng, J. Liu, X. Gu, H. Gong, X. Shi, T. Liu, C. Wang, X. Wang, G. Liu, H. Xing, W. Bu, B. Sun, Z. Liu, *Adv. Mater.* **2014**, *26*, 1886; b) E. S. Olson, T. Jiang, T. A. Aguilera, Q. T. Nguyen, L. G. Ellies, M. Scadeng, R. Y. Tsien, *Proc. Natl. Acad. Sci. USA* **2010**, *107*, 4311; c) K. Li, B. Liu, *Chem. Soc. Rev.* **2014**, *43*, 6570.
[97] a) Y. Song, S. Zhu, S. Xiang, X. Zhao, J. Zhang, H. Zhang, Y. Fu, B. Yang, *Nanoscale* **2014**, *6*, 4676; b) F. Wang, Z. Xie, B. Zhang, Y. Liu, W. Yang, C. Y. Liu, *Nanoscale* **2014**, *6*, 3818.
[98] Q. Fang, Q. Wang, W. Lin, X. You, Y. Dong, Y. Chi, *Sens. Actuators, B* **2017**, *244*, 771.
[99] W. Kasprzyk, P. Krzywda, S. Bednarz, D. Bogdał, *RSC Adv.* **2015**, *5*, 90473.